Title

Investigation of key parameters and issues in simulating centrifuge model tests of a sheet-pile wall retaining a liquefiable soil deposit

Authors

Basu, Devdeep
Pretell, Renmin
Montgomery, Jack
et al.

Publication Date

2022-05-01

DOI

10.1016/j.soildyn.2022.107243

Peer reviewed

Soil Dynamics and Earthquake Engineering 156 (2022) 107243

Contents lists available at ScienceDirect

Soil Dynamics and Earthquake Engineering

journal homepage: www.elsevier.com/locate/soildyn

Investigation of key parameters and issues in simulating centrifuge model tests of a sheet-pile wall retaining a liquefiable soil deposit

Devdeep Basu [a,*], Renmin Pretell [b], Jack Montgomery [a], Katerina Ziotopoulou [b]

[a] Dept of Civil and Environmental Engineering, Auburn University, Auburn, AL, USA
[b] Dept of Civil and Environmental Engineering, University of California, Davis, CA, USA

ARTICLE INFO

Keywords:
Liquefaction
Relative density
Sheet-pile wall
LEAP
Centrifuge model testing
Validation

ABSTRACT

Numerical simulations of centrifuge experiments examining a sheet-pile wall with a liquefiable backfill are conducted and results are compared against the experimental responses to evaluate the numerical tools' ability to accurately predict the seismic performance of this geosystem. The platform FLAC and the constitutive model PM4Sand are used for the simulations, and focus is placed on the sheet-pile wall displacements. The influence of relative density (D_R) on the system's response is evaluated, together with the influence of other parameters such as the soil's permeability and numerical model construction method. The consideration of both mass-based and CPT-based D_R estimates allows for a better prediction of the overall range of permanent sheet-pile wall displacements. Other parameters have a moderate to important effect on the estimated pre-shaking displacements but only a minor to moderate effect on the end-of-shaking wall displacements.

1. Introduction

Earthquake-induced liquefaction of sands poses a major threat to infrastructure as excess pore pressure builds in soils during cyclic loading, resulting in a loss of strength and stiffness, and large deformations. Lateral spreading and settlement due to liquefaction can be significant sources of damage, as observed in past earthquakes such as Kobe (1995) and Christchurch (2011) [1,2] to name a few. Empirical models [3–6] are commonly used to predict lateral displacements and post-liquefaction reconsolidation settlements in engineering practice. However, these models are developed for scenarios with level ground, homogeneous soil deposits, and free-field conditions, and are limited in their ability to assess liquefaction effects in more realistic settings. For scenarios of geotechnical systems that involve soil stratification, soil-structure interaction and other complexities, numerical simulations with nonlinear constitutive models are a more suitable alternative for predicting soil responses and overall geosystem performance.

Numerical predictions are intimately related to the numerical platform used for simulations, the ability of constitutive models to accurately simulate soil behavior, as well as the input parameters, calibration protocols, and various modeling decisions that the analyst must make [7–13]. The calibration of constitutive models is commonly conducted at the element level to reasonably match results from laboratory tests (e.g., cyclic direct simple shear data). The validation of numerical models is commonly conducted at the system-level against well-documented case histories [14] or controlled centrifuge model tests [8,9]. The process of validation helps in identifying the capabilities as well as the limitations of the numerical simulations in capturing failure mechanisms and specific response metrics at the system-level.

Validation exercises commonly place significant attention on the ability of the numerical models to capture all the mechanisms and behaviors of relevance. Particularly for validation exercises against centrifuge model tests, the ability of the latter to match the test design specifications is critical. Common sources of discrepancies in centrifuge model testing, and thus uncertainties in their results, are (i) the achievement and accurate reporting of target geotechnical properties, (ii) the replication of the desired boundary conditions (iii) any unmeasured properties (e.g., shear wave velocity), that may lead to poorly constrained input parameters for the numerical model, and (iv) errors in the expected location of the sensors within the models that later lead to incompatible comparisons against the numerical predictions. These factors can lead to discrepancies between the as-built experimental conditions and the simulations, which makes a fair comparison between the two difficult. For example, physical challenges associated with placement of the sand within the centrifuge container might lead to variations in the soil's relative density (D_R) or inaccuracies in

* Corresponding author.
E-mail address: dzb0048@auburn.edu (D. Basu).

https://doi.org/10.1016/j.soildyn.2022.107243
Received 15 September 2021; Received in revised form 4 February 2022; Accepted 4 March 2022

measurements (e.g., Beber et al. [15]). Differences between the D_R values estimated based on mass and cone penetration test (CPT) measurements are also expected [15]. Moreover, past validation exercises have shown that a well-constrained and measured shear modulus, as opposed to one obtained from empirical and semi-empirical observations, can lead to a significant improvement between experimental observations and numerical simulations [12,16]. Measurements of the permeability of the soil and its possible variations during testing can also be critical for simulating liquefaction [17–20]. Understanding the influence of this range of factors on controlled centrifuge experiments and numerical models can provide valuable insights to engineers and researchers about which ones are more likely to also control the response of geosystems in the field.

The Liquefaction Experiments and Analysis Projects (LEAP) were a series of international collaborative efforts to analyze the dynamic response and liquefaction of soil-structure systems (e.g., Manzari et al. [21] amongst others) with the goal of validating numerical models by producing and utilizing high-quality data from element tests and centrifuge experiments. This paper presents the results from a numerical study performed as part of the LEAP 2020 exercise simulating centrifuge tests of a soil-sheet-pile wall system. The original simulations were performed as part of a "Type B" prediction exercise (i.e., the predictions were made after the experiments had been performed, but the predictors had no knowledge of the results) with sensitivity analyses performed after the experimental results were released. The main objectives of this work are: (1) to establish the ability of the chosen set of numerical tools and modeling protocols to reasonably capture the experimentally observed responses; (2) to investigate the importance of different D_R estimations on the accuracy of the numerical predictions for a soil-sheet-pile wall system; and (3) to study the influence of soil properties as well as modeling decisions on the predicted wall displacements, surface settlements, excess pore pressures, and response spectra. The simulations described herein use the numerical platform FLAC 8.0 [22] and the constitutive model PM4Sand v3.1 [23]. The paper describes the simulation approach, as well as features of the selected numerical platform, constitutive model, and soil properties. Relevant results from laboratory tests are also summarized. The calibrated numerical model is used to perform simulations of the centrifuge model tests, and results are compared against recorded experimental responses [24]. The effects of variations of parameters, such as D_R, on the system response are evaluated to assess the overall efficacy and sensitivity of the selected numerical platform and constitutive model in predicting the centrifuge responses. Lessons from this study and recommendations for simulations involving soil liquefaction and soil retaining structures at the field-scale are discussed.

2. Centrifuge model tests

Simulations are performed for eleven centrifuge tests from the LEAP 2020 exercise [25] (Table 1). Five of these centrifuge tests were performed at the Rensselaer Polytechnic Institute (RPI), two at Ehime University (EU), two at Kyoto University (KyU), and one each at the Korea Advanced Institute of Science and Technology (KAIST), the University of California, Davis (UCD), and Zhejiang University (ZJU). The centrifuge experiments were conducted under an acceleration field that was N_g times larger than the acceleration of gravity (g). This enabled the use of a reduced-scale model to represent a full-scale prototype geotechnical system according to relevant centrifuge scaling laws [26]. The geotechnical system, presented in Fig. 1, is a sheet-pile wall retaining a deposit of liquefiable 'backfill', with a dense layer of sand under the backfill. The same layers are used as a 'toefill' in front of the wall. Both the backfill and toefill consist of Ottawa F-65 sand. Table 1 presents details of the acceleration field and wall properties utilized for each test, whereas Fig. 1 shows the numerical model with its dimensions in prototype scale and the sensor locations. Attention herein is placed on select locations that are described throughout the paper, while results for all locations are described by Basu et al. [27].

Table 1
Centrifuge model tests performed as part of LEAP 2020 prediction exercise.

Centrifuge Facility	Test Number	Centrifugal Acceleration (g)	Sheet-pile wall properties (E = 6.89 GPa, I = 0.0001 m^4)		
			Density (kg/m^3)	Height (m)	Cross-sectional area (m^2)
RPI	9	23	2740	7	0.11
RPI	10	23	2740	7	0.11
RPI	11	23	2740	7	0.11
RPI	12	23	2740	7	0.11
RPI	13	23	2740	7	0.11
EU	2	40	2680	8.5	0.12
KyU	1	40	2710	8.5	0.12
KyU	3	40	2710	8.5	0.12
KAIST	1	40	2720	7.5	0.112
UCD	1	27	2740	7.5	0.11
ZJU	1	26	2800	7.5	0.12

All centrifuge experiments followed similar protocols and recorded the same types of data at similar prescribed locations (Zeghal et al. [25]). The specimen was built in a rigid wall container by placing an aluminum sheet-pile wall to divide the container into two sections (backfill and toefill) and then pluviating the sand. First, a 1 m-thick layer of dense sand with $D_R = 90\%$ was placed, within which the sheet-pile wall was embedded 0.5 m (Fig. 1). Second, a looser layer of sand with $D_R = 65\%$ was placed up to 1 m above the dense layer in the toefill and up to 4 m above the dense sand layer in the backfill. The aluminum sheet-pile wall was embedded 0.5 m into the dense sand layer, and it extended between 2.5 m and 4 m above the backfill surface for the various centrifuge tests. For the centrifuge experiments, the sheet-pile wall extended the full width (8.5 m in prototype units) of the container in the out-of-plane direction. During construction, the sheet-pile wall was fixed to the rigid box to prevent its penetration into the soil underneath and rotation towards the toefill. Pore pressure transducers and accelerometers were installed at various depths in the soil deposit, both behind and in front of the wall, to record excess pore pressures and acceleration time histories. Linear variable differential transformers (LVDTs) were installed at the soil surface to record settlements, and on the sheet-pile wall to monitor lateral displacements during the test (Fig. 1). The displacement sensors $WY\text{-}_T$ and $WY+_T$ and the settlement LVDTs WY- and WY+ were located at the same height on the wall and soil surface, respectively, but on either side of the centerline of the container in the out-of-plane direction. The soil was saturated using a viscous fluid with a viscosity N_g times higher than that of water to ensure consistency between dynamic and diffusion time scaling factors [26]. The centrifuge model was spun up to the target acceleration field in stages. CPT tests were conducted between depths of 1 and 3 m prior to shaking for all the experiments except KyU-1 and KyU-3. The model was then subjected to an input motion applied at the base of the rigid box.

3. Numerical model

The numerical platform FLAC 8.0 [22] is used for the simulations. FLAC is a two-dimensional explicit finite difference program for engineering mechanics computations. The program can simulate the behavior of materials that may undergo plastic flow when their yield limits are reached. Materials are represented by zones, or elements, which form a grid that is adjusted by the user to fit the shape of the structure to be modeled. The behavior at the zone level in response to the applied forces or boundary restraints is guided by a prescribed linear or nonlinear stress-strain (constitutive) law. A mixed-discretization technique with quadrilateral zones is utilized in FLAC, where each quadrilateral zone is divided into two overlaid sets of constant strain triangular subzones. FLAC uses an explicit, Lagrangian calculation

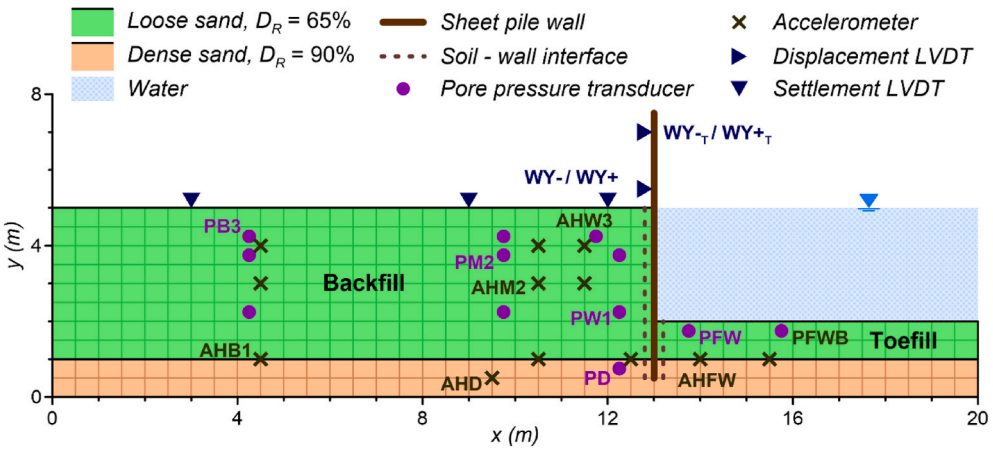

Fig. 1. Geometry of centrifuge model test in prototype scale as represented by the numerical setup in FLAC. The rigid box was not simulated explicitly and is thus not shown. Sensor locations correspond to RPI-9. Sensors WY-$_T$, WY+$_T$, WY-, and WY+ are located on either side of the centerline cross-section in the out-of-plane direction.

scheme which, along with the mixed-discretization zoning technique, ensures that plastic collapse and flow are modeled accurately [22]. The explicit formulation of the program makes it time step- and stress path-dependent, meaning that the estimated results depend on stress initialization procedures and the modeler's numerical choices. FLAC uses a small dynamic time step to obtain an accurate solution, but it is typically prudent to explore smaller time steps and ensure stability of results.

The nonlinear constitutive model used for these simulations is PM4Sand Version 3.1 [23] which has been developed to model the behavior of sands and non-plastic silts in earthquake engineering problems. PM4Sand is a plane strain stress ratio-controlled, critical state-compatible, bounding surface plasticity model, which is an extension of the plasticity model initially developed by Dafalias and Manzari [28] and is described by Boulanger and Ziotopoulou [23]. It is cast in terms of the relative state parameter, ξ_R [29], such that the soil properties can change during the simulation as a function of changes in state (i.e., changes in mean effective stress or void ratio or both). The model requires three primary input parameters, 21 secondary parameters, the atmospheric pressure (P_a) which sets the units, and two flags. The model is developed such that it can be used given the three primary parameters, while all secondary parameters have been calibrated by the developers to reasonably approximate the range of behaviors exhibited by the broader body of data on clean sands. The secondary parameters can always be modified to better capture observed behaviors when soil-specific laboratory tests or any other data are available.

3.1. Calibration of constitutive model

The constitutive model calibration for this study is performed through single-element simulations of undrained cyclic stress-controlled direct simple shear (DSS) tests to reasonably capture behaviors measured in these tests. The primary PM4Sand model parameters calibrated in this study are the D_R, the shear modulus coefficient (G_o), and the contraction rate parameter (h_{po}). D_R controls the relative state of the soil and thus its contractive or dilative behavior, G_o relates to the shear wave velocity and controls the small-strain stiffness, and h_{po} controls the soil's contractiveness and through that its cyclic strength. Additionally, the n^b parameter, which controls the bounding ratio and thus the peak effective friction angle, is also calibrated in this study, along with maximum void ratio (e_{max}), minimum void ratio (e_{min}), and critical state friction angle (φ'_{cv}) which are assigned values informed by relevant Ottawa-F65 data [12,16]. Default values reported in Boulanger and Ziotopoulou [23] are used for all other PM4Sand parameters.

For the current study, D_R is estimated based on (i) the mass of sand used during pluviation for the Type B simulations and (ii) correlations with CPT data by Bolton et al. [30], as part of the sensitivity studies. Sepulveda et al. [31] found this correlation to fit well with the data from LEAP. The Bolton et al. [30] correlation is outlined in equation (1):

$$D_R = 0.2831\left(\frac{q_c - \sigma_v}{\sigma'_v}\right) + 32.964 \quad (1)$$

where, D_R is in percentage, q_c is the measured cone tip resistance, σ_v is the total vertical stress, σ'_v is the effective vertical stress.

The values for G_o are selected by using the PM4Sand functional form [23] with a slight modification (Equation (2)) to better match the shear wave velocity data for Ottawa F-65 sand [24] and therefore the maximum shear modulus G_{max}:

$$G_o = 10.606\,(D_R) - 229 \quad (2)$$

where, D_R is in percentage. This relationship is only valid for D_R values between 50% and 90%. The parameter h_{po} is calibrated for a given D_R (Table 2) to reach a double amplitude shear strain of 6% in 15 loading cycles at the cyclic stress ratio (CSR) established by the triggering curve (Fig. 2). A triggering curve is developed for the h_{po} calibration by fitting the available cyclic strength data on Ottawa F-65 sand [32–38] and numerical simulations [16] using a similar relationship to the one by Idriss and Boulanger [39] (Fig. 2). It must be noted that this curve attempts to capture the overall behavior by honoring trends of the combined data set and not to match any single point. The cyclic strength data in Fig. 2 correspond to an effective confining pressure of 100 kPa, which is higher than the average effective stress in the simulations (around 40 kPa). Since cyclic strength data for Ottawa F-65 at lower effective confining pressures are not available for the full range of D_R values considered, the calibration of h_{po} was performed at a confinement of 100 kPa for this study. PM4Sand has been developed and shown to effectively capture the effects of confining pressure on liquefaction triggering without additional calibration [23]. This was checked by comparing the results from cyclic DSS simulations using the proposed calibration with the experimental data from El Ghoraiby et al. [24], which was performed at a confinement of 40 kPa for sand at a D_R of 67%. The curve from the simulation is in good agreement with the experimental data between 15 and 25 cycles, but additional experimental data is needed to judge the applicability of the calibration at lower stresses for the full range of D_R considered in this study. The n^b parameter is assigned a value of 0.6 to match the rate of strain accumulation for Ottawa F-65 sand as suggested by a previous study on a similar problem [40]. The critical state friction angle φ'_{cv} is reduced to 30° from the PM4Sand default value of 33° to better match the slope of the frictional

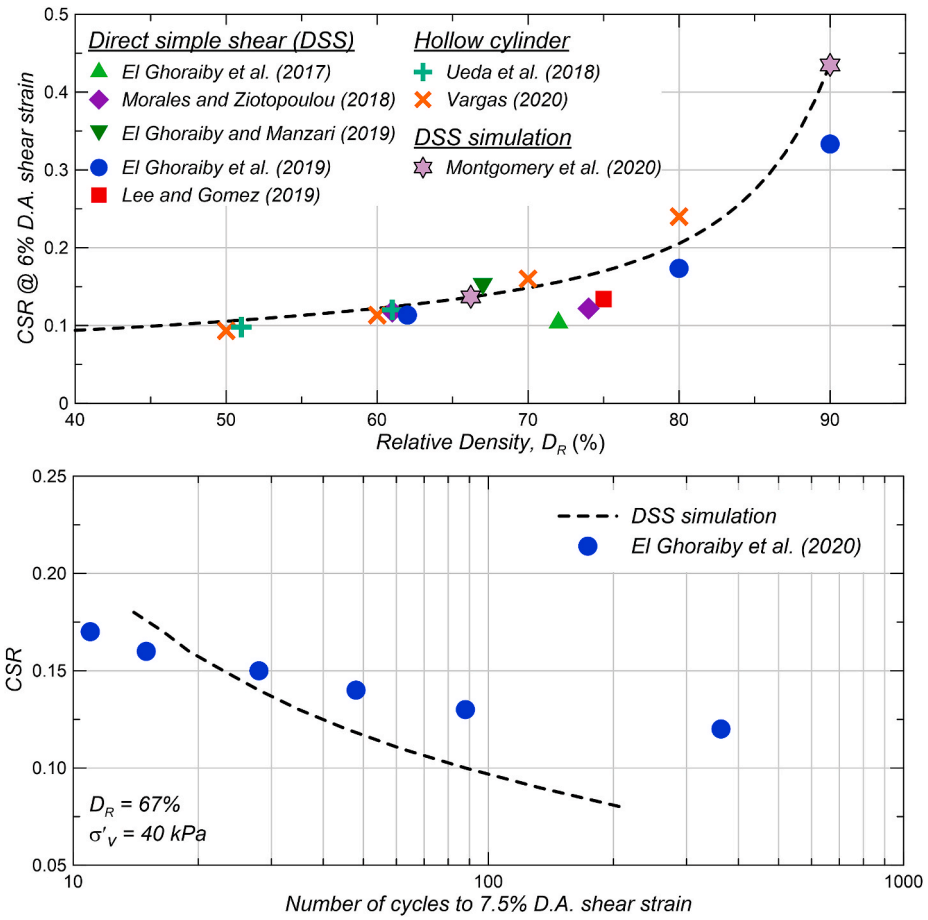

Fig. 2. Triggering relationship for Ottawa F-65 sand used for calibration of the PM4Sand parameters (top) and a comparison of a calibrated direct simple shear (DSS) simulation and laboratory test results from El Ghoraiby et al. [24] at 40 kPa for Ottawa F-65 sand at a D_R of 67% (bottom). The cyclic stress ratio for the triggering relationship corresponds to 6% double amplitude shear strains in 15 cycles and all data in the upper figure is for an effective stress of 100 kPa.

envelopes (bounding line) of the stress path plots from the cyclic DSS tests [16]. A friction angle of 30° for Ottawa F-65 sand is also consistent with the results reported by Parra Bastidas [41] based on work by others [42–49].

3.2. Input motions

The centrifuge models are subjected to horizontal ramped sinusoidal input motions applied at the base of the model as accelerations with peak values varying from 0.15g to 0.18g. These input motions are the same as those used recorded on the model container during the centrifuge experiments. At some of the centrifuge facilities, an additional

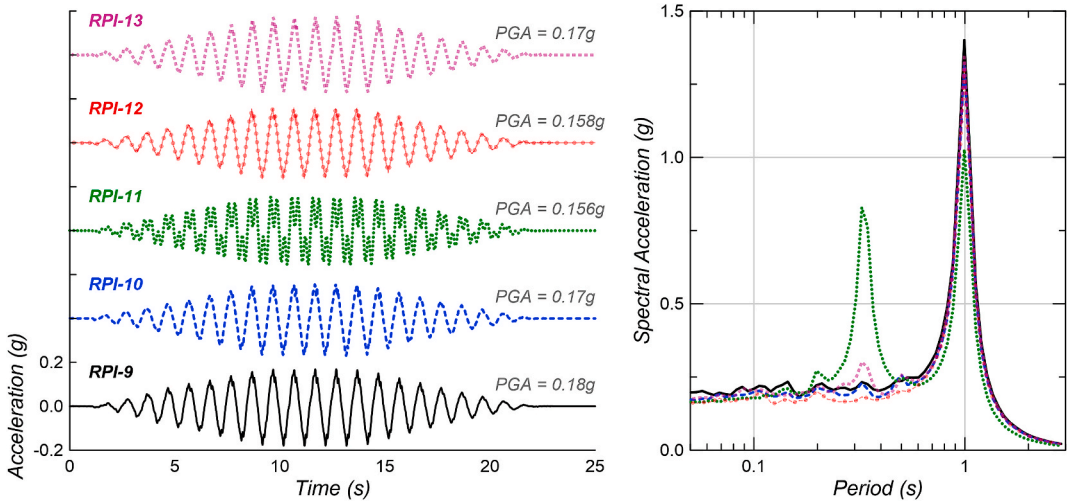

Fig. 3. Acceleration time histories and response spectra (5% damped) for the horizontal components of the RPI input motions.

vertical motion component was recorded with a peak amplitude approximately 10 times smaller than the horizontal component and is also applied at the base of the model. Fig. 3 shows the response spectra and acceleration time histories of the horizontal input motion components used for the centrifuge tests performed at RPI. The RPI motions have similar peak accelerations and a predominant frequency around 1 Hz; the RPI-11 motion has an additional high-frequency component at around 3 Hz (or 0.3 s).

3.3. Numerical model

The numerical models consist of square zones with a dimension of 0.5 m by 0.5 m to represent the dense layer, toefill, and backfill. With this zone size, the model is expected to be able to propagate wavelengths greater than 4 m or frequencies less than 37 Hz (Kuhlemeyer and Lysmer [52]). The sheet-pile wall is modeled in FLAC using elastic beam elements with the properties provided by each centrifuge facility (Table 1) and nodes at every 0.5 m to match the soil discretization. The thicknesses of the sheet-pile walls used in the experiments were small and varied between 5 and 10 cm in prototype units. Therefore, the simulations do not explicitly model the wall thickness, but the thickness is used to specify the sheet-pile wall properties (Table 1). These properties are internally utilized by FLAC to compute wall displacements. The sheet-pile is connected to the soil using unbonded interfaces at both sides to simulate the friction between these two materials while allowing for separation and slippage. The simulations use a soil-wall interface friction angle of 30° which is equal to the critical state friction angle of the soil. Early simulations indicated that using smaller interface friction angles result in numerical instabilities. The normal and shear stiffnesses for the interface are both set to 3.4 GPa, which is approximately equal to 10 times the stiffness of the surrounding soil, as recommended in the FLAC User Manual [22]. Large deformations are enabled for all simulations to update the node coordinates as the model geometry progressively changes according to the Lagrangian scheme. FLAC calculates a default time step to ensure solution stability based on the soil stiffness, permeability, and zone size. For these simulations, a time step of 10^{-5} s, which is smaller than the recommended timestep is used to ensure consistency between the different simulations. Sensitivity analyses show that using a smaller zone size or time step resulted in negligible differences in the final wall displacement (less than 5%), as discussed later.

During the stress initialization phase, the modeling procedure follows closely the prototype conditions and model construction. The analyses do not explicitly simulate the rigid box that surrounds the soil, but the constraints the box imposes on the geosystem are applied as mechanical boundary conditions. All nodes at the bottom of the model are fixed in both the horizontal and vertical directions while all the side nodes are fixed only in the horizontal direction. The reported centrifugal spinning accelerations from each facility are used to establish the pre-shaking conditions by constructing the soil deposit in layers across all the deposit and then excavating the soil in front of the sheet-pile wall. During this phase, a gravity acceleration of $1/N_g$ is used to simulate the prototype conditions, and the soil is assigned the Mohr-Coulomb model with the critical state friction angle and a cohesion of 4 kPa. This cohesion is used to ensure numerical stability at the toe of the wall and is common practice in numerical simulations (e.g., Guan and Madabhushi [53]). Once the static stresses are established, the pore pressure is applied on the nodes to establish a water table elevation of 5 m (Fig. 1). The appropriate pressure on the top boundary of the toefill area and on the front side of the sheet-pile wall is applied to establish submerged conditions. Saturation is set to 100% across the model and equilibrium of pore pressures is established. Water flow is allowed along the top surface of the model, whereas flow across the container boundaries and wall is restricted. Pore pressures and saturation are fixed at the top nodes to allow for free drainage along the top surface. Thereafter, gravity is increased in increments of $1/N_g$ to approximate the centrifuge spinup process, allowing the prototype stresses to establish without arching or boundary effects. The effect that the selected construction method and the constitutive model used during the construction stage have on the estimated seismic-induced displacements is discussed later in the paper.

Following the static stress initialization, the dynamic phase of the simulation is conducted. The PM4Sand model is assigned to the dense and the liquefiable sand layers, and Rayleigh damping is set to 0.5% centered at the fundamental frequency of the input motion of 1 Hz. A local damping of 5% is assigned to the sheet-pile wall, and the horizontal input motions are applied as accelerations at the base and the sides of the model. When available, time histories of vertical accelerations are also applied to the base of the model. The shaking is continued for the duration of the recorded event for each test (approximately 22 s). After the end of shaking, the base of the model is brought to a zero-velocity condition by applying both horizontal and vertical decelerations to the bottom boundary of the model. These decelerations are opposite in direction to the average velocities along this boundary and the magnitude is calculated to reduce the average velocity to zero in 0.2 s. This procedure is meant to approximate the gradual stopping of dynamic shaking in the centrifuge and thus to avoid sudden changes in velocity within the model. After the base of the model is brought to a zero-velocity condition, the model is allowed to reconsolidate under its own weight. Results from the post-shaking phase are discussed by Basu et al. [27] and not included herein as the additional settlement and displacements after the end of shaking were small relative to the dynamic phase in these simulations.

The numerical simulation protocol used for the analyses does not allow for rocking of the container to be replicated. Some of the simulations are conducted considering both the horizontal and vertical input motions, however, significant rocking is not expected to have occurred during the experiments anyways as the vertical motion amplitudes are 10 times smaller than the horizontal motion amplitudes. Therefore, the inability to numerically model rocking is unlikely to have a notable effect on the predictive capability of the simulations.

4. Simulation results

Results from the baseline simulations and sensitivity studies are presented in four parts: (1) a focused discussion on the RPI-9 simulation results, considered as baseline for comparison purposes; (2) an evaluation of the effect of D_R across multiple centrifuge experiments; (3) an evaluation of the effect of the soil's permeability and its potential variation during shaking; and (4) the effects of modeling decisions made throughout the simulation process, including model construction method, the constitutive model used for stress initialization, the sheet-pile wall interface properties, the mesh discretization, and the dynamic time step. Results and comparisons are presented in terms of the sheet-pile wall displacements at locations WY-$_T$ and WY+$_T$ (Fig. 1), surface settlements near the wall at locations WY- and WY+, and excess pore pressures and response spectra at various locations within the model.

4.1. Baseline results for RPI-9

The baseline simulation is conducted for the RPI-9 centrifuge test using best-estimate parameters and following common simulation practices. The baseline scenario considers mass-based D_R (Table 2), constant permeability, model construction conducted by placing soil layers followed by excavation and placement of sheet-pile wall, both model construction and spinup stages using the Mohr-Coulomb constitutive model for sands, baseline properties for the sheet-pile wall interface selected (i.e., using the critical state friction angle and the soil stiffnesses based on the recommendations by Itasca [22] and, zone dimensions of 0.5 m by 0.5 m, and a time step of 10^{-5} s.

The results for the baseline scenario are presented in Figs. 4–7 in terms of soil and wall displacements, surface settlements, excess pore pressures, and acceleration response spectra, respectively. The

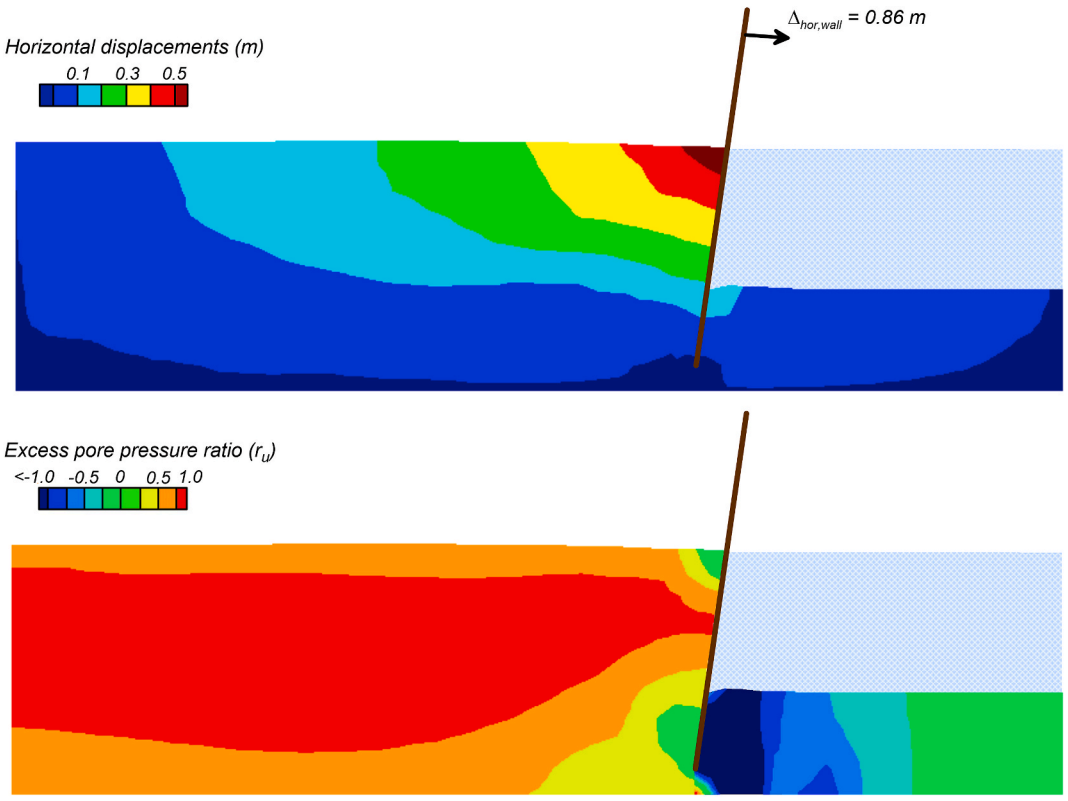

Fig. 4. Contours of horizontal displacements and excess pore pressure ratios at the end of shaking for RPI-9.

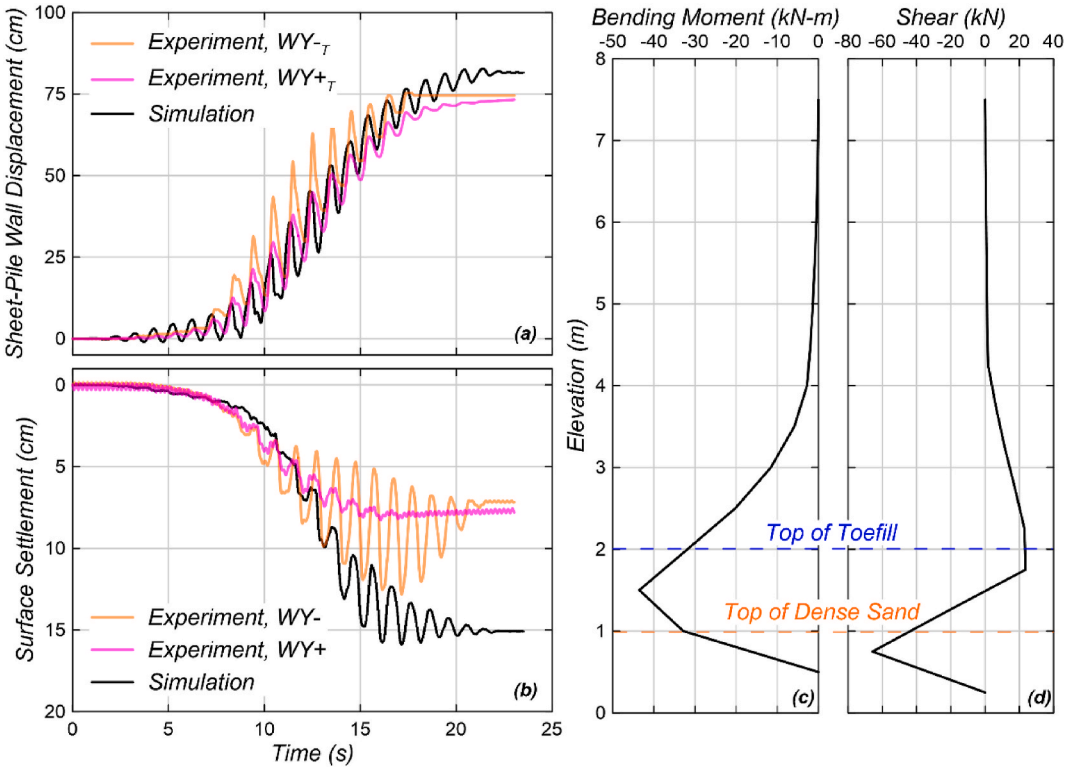

Fig. 5. Sheet-pile wall responses during shaking for RPI-9 for (a) displacement; and (b) surface settlement and at the end of shaking for (c) bending moment and (d) shear in the structural elements. The shear force is plotted at the center of element, while bending moments are plotted at the nodes on each end.

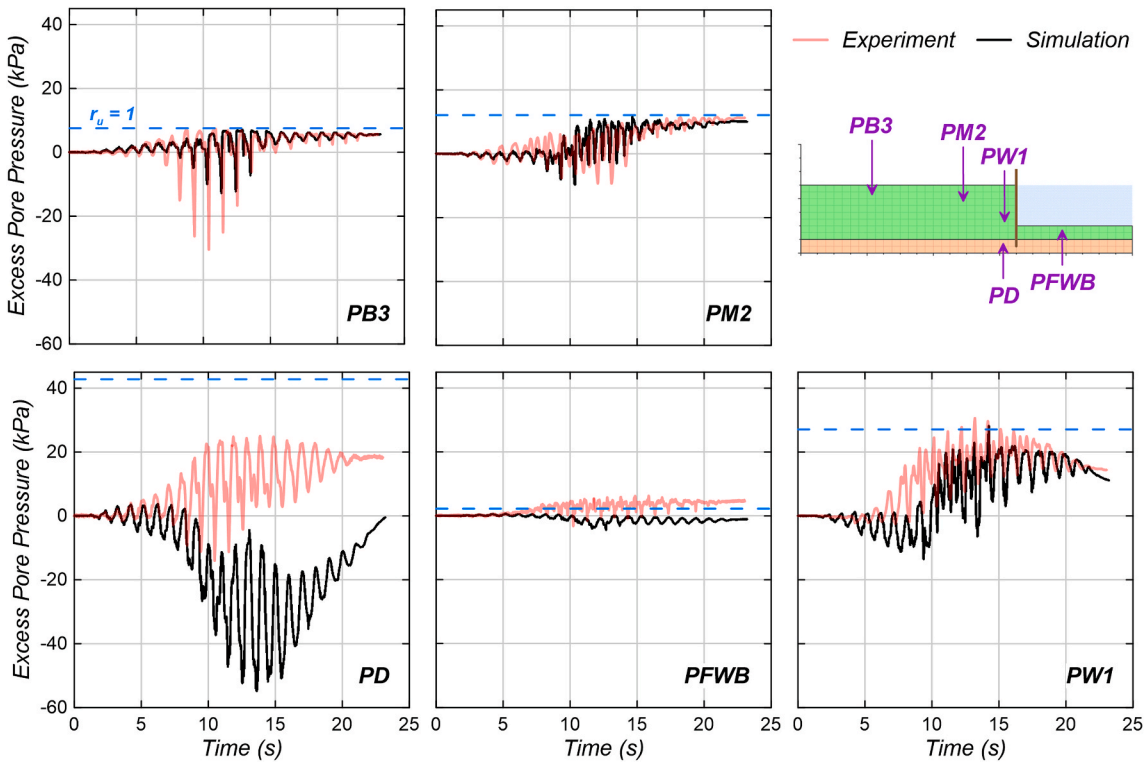

Fig. 6. Excess pore pressure time histories for RPI-9 at various locations indicated in the top right corner.

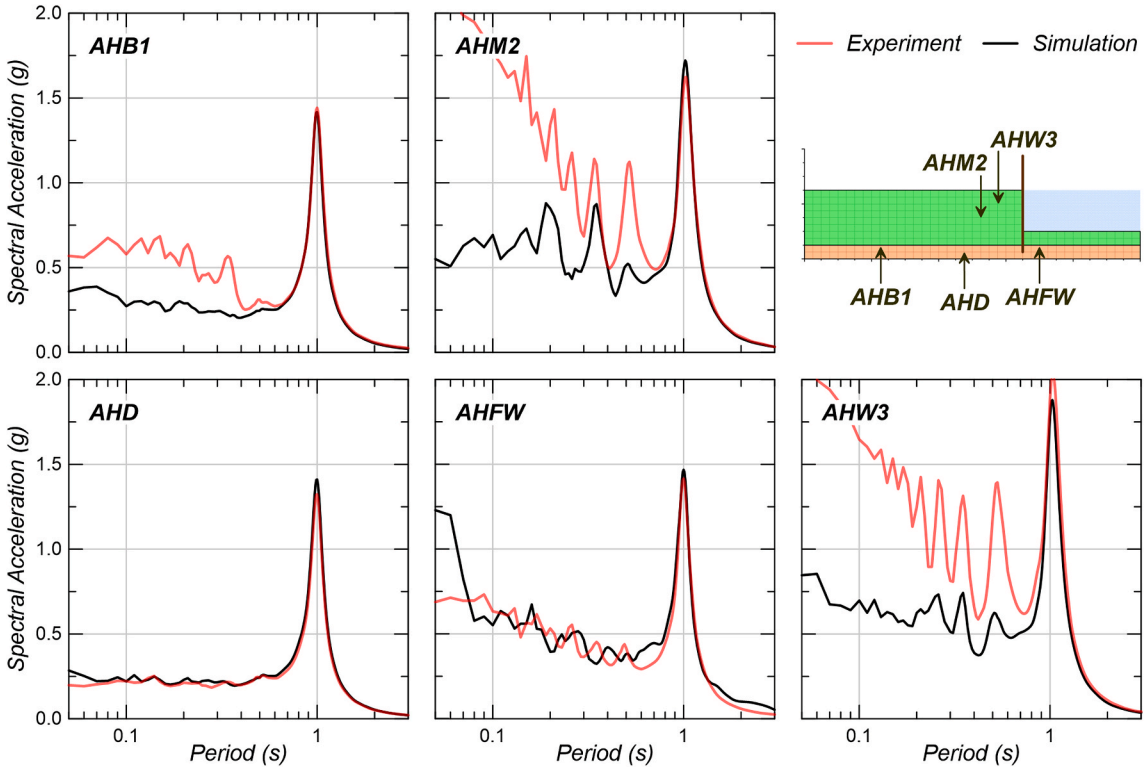

Fig. 7. Response spectra (5% damped) for RPI-9 at various locations indicated in the top right corner.

maximum soil horizontal displacements occur at the soil surface near the sheet-pile wall, with values as high as 50 cm, which decrease towards the left side of the model down to negligible displacements near the rigid box (Fig. 4). The sheet-pile wall moves towards the unconfined area resulting in heave of some of the toefill sands. Excess pore pressure ratios (r_u) at the end of shaking (Fig. 4) show liquefaction was triggered within most of the liquefiable backfill, while dilation (negative excess pore pressures) are observed near the top and base of the wall and throughout

the toefill. The estimated wall displacements are higher than the displacements measured in the experiments by about 8 cm (Fig. 5), which represents a 10% of overprediction, whereas the estimated surface settlements behind the wall are higher than the measured settlements by approximately a factor of two (Fig. 5). The internal bending moment and shear force are also shown in Fig. 5 for the structural elements in the sheet-pile wall. No experimental measurements were collected to compare these internal forces too, but the patterns are consistent with expected patterns for a cantilever retaining wall.

Time histories of excess pore pressures (Fig. 6) indicate that the simulations capture reasonably well the trends and residual excess pore pressure at sensor PB3 and PM2, located in the backfill away from the wall, with exception of the dilation spikes observed at PB3. The predicted and measured excess pore pressures at PW1 follow the same overall trend, however with some observable differences attributed to soil-structure interaction effects such as alteration of the translational component of accelerations near the sheet-pile wall [54] that are not adequately captured in the simulations. Unlike the experimental results, the simulations show dilation within the dense sand at locations PD and PFWB, located near the toe of the wall and at the toefill respectively. The reasons for this disagreement are unclear, but the dilation at this location is present in all of the numerical simulations, including the sensitivity studies shown later. Possible reasons for this discrepancy include suppressed dilation due to friction on the side walls of the centrifuge container, water flow into this zone from out of plane directions (i.e., radial flow), or a lower achieved D_R in this layer.

The estimated and the measured spectral accelerations show good agreement around the input motion's predominant frequency of 1 Hz (Fig. 7). At shorter periods, discrepancies are observed as the high-frequency dilation spikes observed in the experiment near the top of the backfill are not captured. Similar trends in excess pore pressures and response spectra are observed in simulations of the other centrifuge tests [27], and previous LEAP studies [55]. Tsiapas [56], based on sensitivity analyses on liquefiable deposits, found that simulated high-frequency spikes are controlled by the amount of Rayleigh damping assigned to dry soil layers. A Rayleigh damping of 2% anchored at the predominant

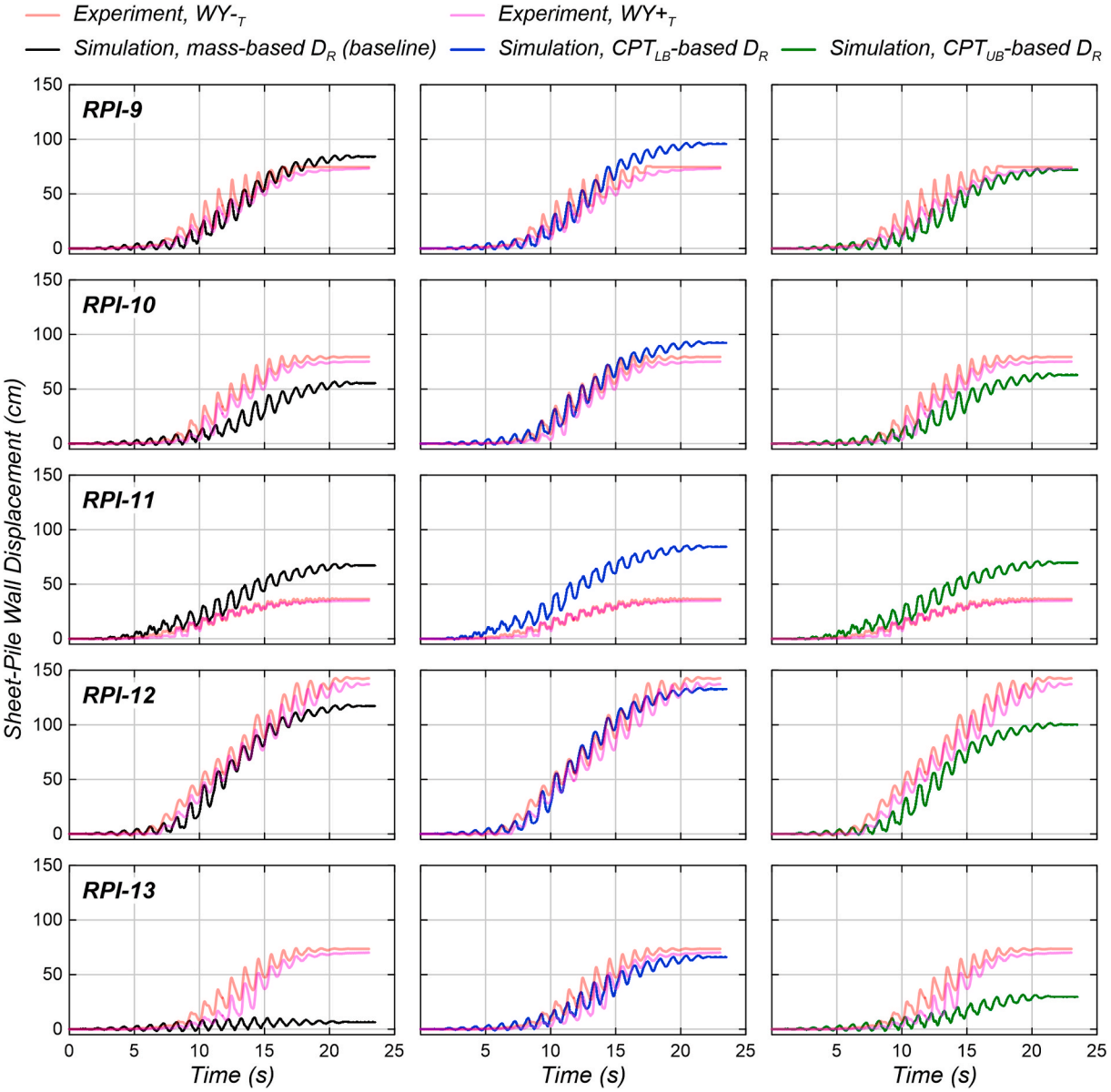

Fig. 8. Comparison between recorded and simulated sheet-pile wall displacement time histories at locations $WY-_T$ and $WY+_T$ for the RPI tests. Each column corresponds to a different approach for estimating the applicable D_R: left column for mass-based D_R, middle column for D_R based on lower bound CPT data, and right column for D_R based on upper bound CPT data.

frequency of the ground response was observed to eliminate the high-frequency spikes using both an elasto-plastic Mohr-Coulomb model and the plasticity model, NTUA-SAND (Papadimitriou et al. [57]). Tsiapas and Bouckovalas [58] extended the work by Tsiapas [56] and found that a similar trend was applicable for saturated soil layers, although to a lesser extent. Their study indicates that other aspects such as the choice of constitutive model, model dimensions, mesh discretization, input motion type, and free field boundary conditions, did not influence the high-frequency content of simulated responses.

4.2. Effect of D_R across centrifuge experiments

The D_R of the liquefiable soil is one of the three primary parameters of the constitutive model used in the simulations and is thus expected to have an important effect on the predicted sheet-pile wall displacements. The baseline scenario uses the mass-based D_R, however, it can also be estimated using CPT data and correlations such as those proposed by Bolton et al. [30] and used by Sepulveda et al. [31]. Herein, the impact of using either the mass-based or CPT-based D_R on the sheet-pile wall displacements, surface settlements, excess pore pressures, and response spectra is studied, and results are presented in Figs. 8–13. The five RPI tests are mainly considered for this investigation as they share the same experimental setup, similar input motion peak accelerations (Fig. 3), and on-site practices and quality control for model preparation. Differences amongst the RPI test are mostly attributed to D_R with the exception of RPI-11, which used a different input motion (Fig. 3).

4.2.1. Effect of D_R on the sheet-pile wall displacements

Three D_R scenarios are considered: one corresponding to the D_R measured based on the mass of sand used during pluviation (mass-based D_R), and the other two based on CPT measurements [31] (CPT-based D_R). Most of the CPT measurements exhibit a non-uniform tip resistance and thus the lower (CPT_{LB}-based D_R) and upper (CPT_{UB}-based D_R) bounds are considered for the analyses (Table 2). The difference between these upper and lower bounds is 5–6% for the RPI tests and as high as 23% for other tests. No CPT data are available for the experiments KyU-1 and -3.

Results in terms of the sheet-pile wall displacements are presented in Figs. 8–10. A comparison of the sheet-pile wall displacements estimated using the three D_R values along with the experimental data is presented in Fig. 8. The most accurate predictions, based on the magnitude of permanent displacements, are obtained using the CPT_{UB}-based D_R for tests RPI-9 and RPI-10, the CPT_{LB}-based D_R for tests RPI-12 and RPI-13, and either the mass-based or CPT_{UB}-based D_R for RPI-11. For RPI-9 and RPI-10, the experimental results are enveloped by using the three D_R estimates, whereas the simulations always underestimated the displacements for RPI-12 and RPI-13 and overestimated the displacement for RPI-11. Fig. 9 shows the effect of D_R on normalized wall displacements, i.e., displacements divided by the wall height. For the experimental results, the trend indicates an overall inverse relation between D_R and the magnitude of displacements, which is reasonable given that the other model parameters and input motions are similar. RPI-13 stands out as a possible outlier from this trend. A linear trend between D_R and the magnitude of displacements is observed in the case of the numerical results.

It is interesting to note that the experimental results for RPI-11 and RPI-13 significantly deviate from other tests' experimental and numerical results. The displacements measured in RPI-11 are approximately half of those from RPI-9 and RPI-10 despite all three having similar D_R. The main difference between these experiments is the higher frequency component in the input motion and a reduction in the PGA (Fig. 3). These variants appear to have led to reduced displacements in the experiment, but do not significantly affect the numerical displacements. Meanwhile, the simulated displacements for RPI-13 for the scenario with mass-based D_R are approximately 90% lower than the measured values. For RPI-13, the CPT measurements indicate the achieved D_R was lower than the targeted value of 75% (Table 2), which may account for some of this discrepancy. Predicted sheet-pile wall displacements for RPI-13 for the scenario with CPT_{LB}-based D_R are only about 8% less than the measured value, indicating good agreement.

Comparisons against results from other centrifuge tests are presented in Fig. 10. The displacement normalization is assumed to reasonably remove the effect of differences in sheet-pile wall heights and thus allow for a fair comparison of results. For the mass-based D_R scenario, the simulated wall displacements are reasonably accurate for RPI-9, ZJU-1, and KyU-1, whereas the predictions improved significantly for tests RPI-10, RPI-12, RPI-13, and EU-2 by using CPT-based D_R, particularly CPT_{LB}-based D_R (RPI-12 and RPI-13). The scenarios with CPT-based D_R do not improve predictions for UCD-1 and KAIST-2. Overall, it is observed that the numerical predictions of wall displacements for all eleven tests are within 50–200% (i.e., a factor of 2) of the corresponding experimental displacements, utilizing either the mass-based D_R or a D_R value falling within the range estimated from the CPT correlation. This level of uncertainty is similar to the observations from other numerical predictions such as liquefaction-induced free-field settlements [59]. Table 3 presents goodness of fit statistics for the normalized displacements. The CPT_{LB}-based D_R has a slightly better R^2 value than the other two scenarios, as well as a lower mean squared error (MSE) and bias, calculated

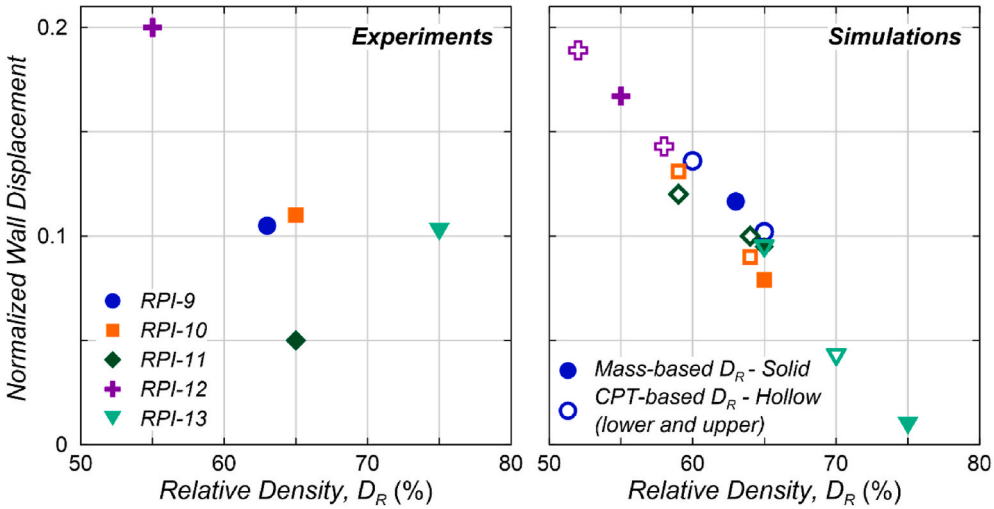

Fig. 9. Normalized sheet-pile wall displacement versus relative density, D_R, for experiments and simulations corresponding to the RPI tests. For the simulations, the solid symbols correspond to the mass-based D_R values while hollow symbols correspond to lower and upper bounds of CPT-based D_R values.

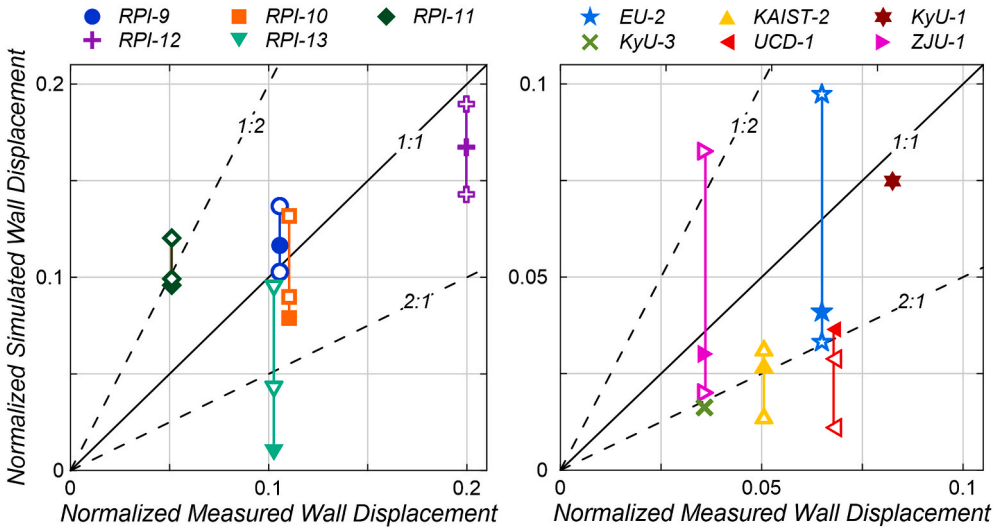

Fig. 10. Normalized sheet-pile wall displacements at locations WY_{-T} and WY_{+T} for all the centrifuge tests. Solid symbols correspond to the mass-based D_R values while hollow symbols correspond to lower and upper bounds of CPT-based D_R values. *Note: No CPT data are available for KyU-1 and KyU-3.*

as the ratio of observed to simulated normalized wall displacement. This indicates that the CPT_{LB}-based D_R was more representative of the soil response observed in the centrifuge experiments than either the mass-based or CPT_{UB}-based D_R values. This reinforces the value of collecting CPT data as part of centrifuge studies [60].

4.2.2. *Effect of D_R on other seismic performance metrics*

Results for surface settlements near the sheet-pile wall, excess pore pressures near the wall at mid-depth, and response spectra near the wall, are presented in Figs. 11–13 for RPI-9 through 13 and the three D_R scenarios described in the previous section. The results suggest a significant impact of D_R on surface settlements, with higher D_R leading to lower surface settlements. The magnitude of settlements is generally in good agreement with the trends observed for the wall displacements, although with an overall tendency for overpredictions and mild underpredictions for RPI-12 and RPI-13. The excess pore pressure is not significantly affected by changes in D_R except for RPI-13, where the measured excess pore pressures go from positive to negative as the D_R changes from 70% (CPT_{UB}-based D_R) to 75% (mass-based D_R). The excess pore pressures from the CPT_{LB}-based D_R are in the best agreement with the experimental results for RPI-13 as they were for wall displacements. The response spectra are less sensitive to changes in D_R, particularly the predominance of the input motion fundamental frequency is preserved for all three scenarios (Fig. 13).

4.3. *Effect of permeability*

All previous simulations used a permeability estimated for Ottawa F-65 sand [24] that was held constant throughout shaking. According to previous studies, permeability can increase after the onset of liquefaction as soil grains lose contact with one another [19,61,62] and can decrease during the post-liquefaction reconsolidation process as the grain contacts are re-established [17,18,63]. For instance, Shahir et al. [63] observed an increase in permeability by a factor of 20 during liquefaction for Nevada sand. Ueng et al. [64] and Bayoumi et al. [65] observed increases in factors of 1.5 and 5-fold during centrifuge tests on Ottawa C-109 and Vietnam sands, respectively. On the contrary, Adamidis and Madabhushi [66], examined centrifuge experiments on Hostun sand and suggested that permeability can increase at most by a factor of 1.2 and such an increase occurs only at effective stresses less than 0.1 kPa. Recent work by Basu et al. [67] has suggested that some of these differences in results from previous studies may be due to soil-specific effects and they found that the magnitude of permeability increase due to liquefaction correlates well with the effective grain diameter (D_{10}) of the soil. In this study, the baseline test RPI-9 is revisited to investigate the effects of increased permeability during liquefaction using the relationship between permeability and excess pore pressure ratio (r_u) proposed by Shahir et al. [63] (Equation (3)):

$$k_m/k_i = \begin{cases} 1 & ; r_u \le 0 \\ 1 + (\alpha - 1) \times r_u^{\beta_1} & ; r_u \le 1 \\ \alpha & ; r_u > 1 \end{cases} \quad (3)$$

where, k_m is the modified permeability, k_i is the initial permeability at $r_u = 0$, α is the factor by which permeability increases at $r_u = 1$, and β_1 controls the rate at which permeability increases with r_u.

Two scenarios of higher permeability at $r_u = 1$ are considered. The first scenario, HP_1, consists of permeability increases up to a factor $\alpha = 5$, whereas the second, HP_2, up to a factor $\alpha = 20$ the original baseline permeability. The factor of 5 for Ottawa F-65 sand is selected based on a correlation between effective grain diameter (D_{10}) and α developed from simulation of centrifuge and shake table experiments [67] whereas the factor of 20 is based on the recommendations by Shahir et al. [63]. A $\beta_1 = 1$ is used in this study, as Shahir et al. [63] showed that it leads to reasonable results.

The simulated results suggest that some amount of drainage, and thus excess pore pressure dissipation, occurs along with an increment of generation of excess pore pressure during shaking, which is consistent with other investigations [68]. Additional excess pore pressure dissipation may occur due to radial drainage in the experiments, but this mechanism is not reflected in the 2D simulations. Overall, the excess pore pressure at PW1, near the wall, is lower for HP_2 than HP_1, and these two are lower than the excess pore pressures of the baseline scenario (Fig. 14). Usually, the rate of excess pore pressure generation is much higher than dissipation in the early stages of earthquake loading when the shaking amplitude is high. Thus, there is an overall increase in excess pore pressures. The dissipation, however, is higher if permeability increases by an order of magnitude or more, such as observed in the HP_2 scenario. In HP_2, significant pore pressure dissipation is observed towards the end of shaking at PB3, near the ground surface away from the wall, which ultimately leads to excess pore pressures lower than in the baseline scenario. These results indicate that using a variable permeability model with $\alpha = 5$ or a constant permeability model leads to reasonable results, but using a larger α leads to excessive dissipation of excess pore pressures during shaking. This observation agrees with the reported α value of 5 for Ottawa F-65 sand by Basu et al. [67] and

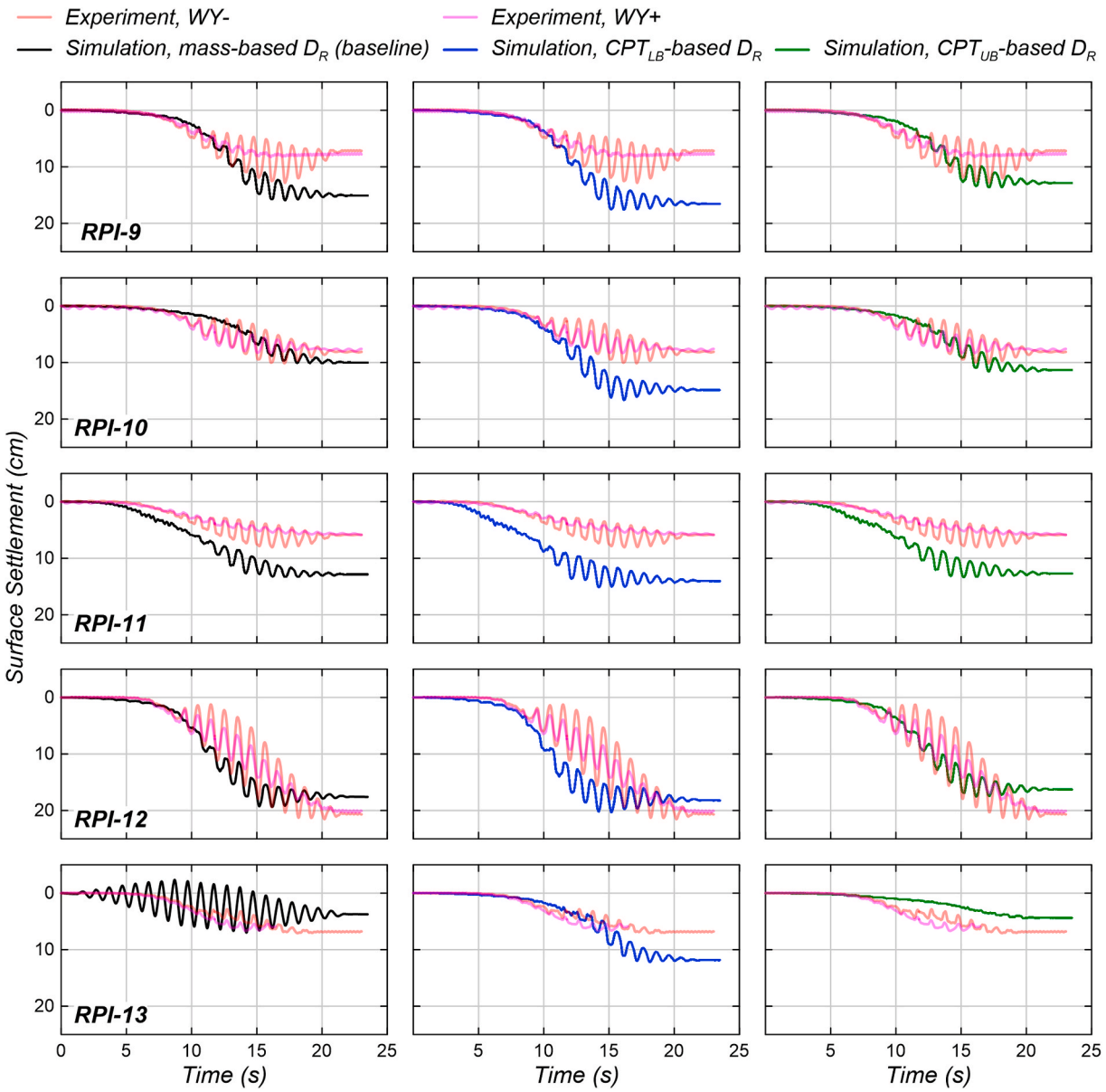

Fig. 11. Surface settlements at locations WY- and WY+ for all the RPI tests. Each column corresponds to a different approach for estimating D_R: left column for mass-based D_R, middle column for D_R based on lower bound CPT data, and right column for D_R based on upper bound CPT data.

highlights the need for soil-specific calibration when using variable permeability models.

The results in terms of sheet-pile wall displacements and surface settlements are observed to be less sensitive to variations in permeability (Fig. 14). For the HP_1 scenario, the estimated displacement is only 4% higher than those from the baseline simulation, whereas it decreases by about 15% for HP_2. The differences in surface settlement behind the wall are negligible among all three scenarios. These results agree with the observations by Basu et al. [67] that using a variable permeability model can improve predictions of excess pore pressure dissipation and settlement rate, but has a smaller effect on the overall magnitude of settlements.

4.4. *Effect of modeling decisions*

The previous sections focused on the effect of variations in D_R and permeability on the seismic response of the soil-sheet-pile wall system. However, there are many decisions that must be made by a modeler when creating a simulation that are not commonly explored to see their effect on the final results. In this section, the effects of some of these modeling decisions on the wall displacements are investigated. These modeling decisions include: (1) the model construction method; (2) the soil constitutive model used during model construction and spinup; (3) the sheet-pile wall's interface stiffness and friction angle; and (4) the mesh discretization (zone dimensions) and time step used during shaking. These investigations are conducted for the RPI-9 test and results are compared against the measured and numerical results from the baseline scenario in terms of sheet-pile wall displacements.

4.4.1. *Effect of model construction process*

The baseline scenario considers the following model construction which follows a hypothetical field application: (1) placement of layers of sand in the rigid box up to a height of 5 m both behind and in front of the wall; (2) creation of the sheet-pile wall; and (3) excavation of the sand in front of the wall. The effect of using an alternative construction process, which is more consistent with the procedure used at the centrifuge facilities is investigated in this section. This alternative construction process consists of: (1) placement of the dense layer in the rigid box; (2)

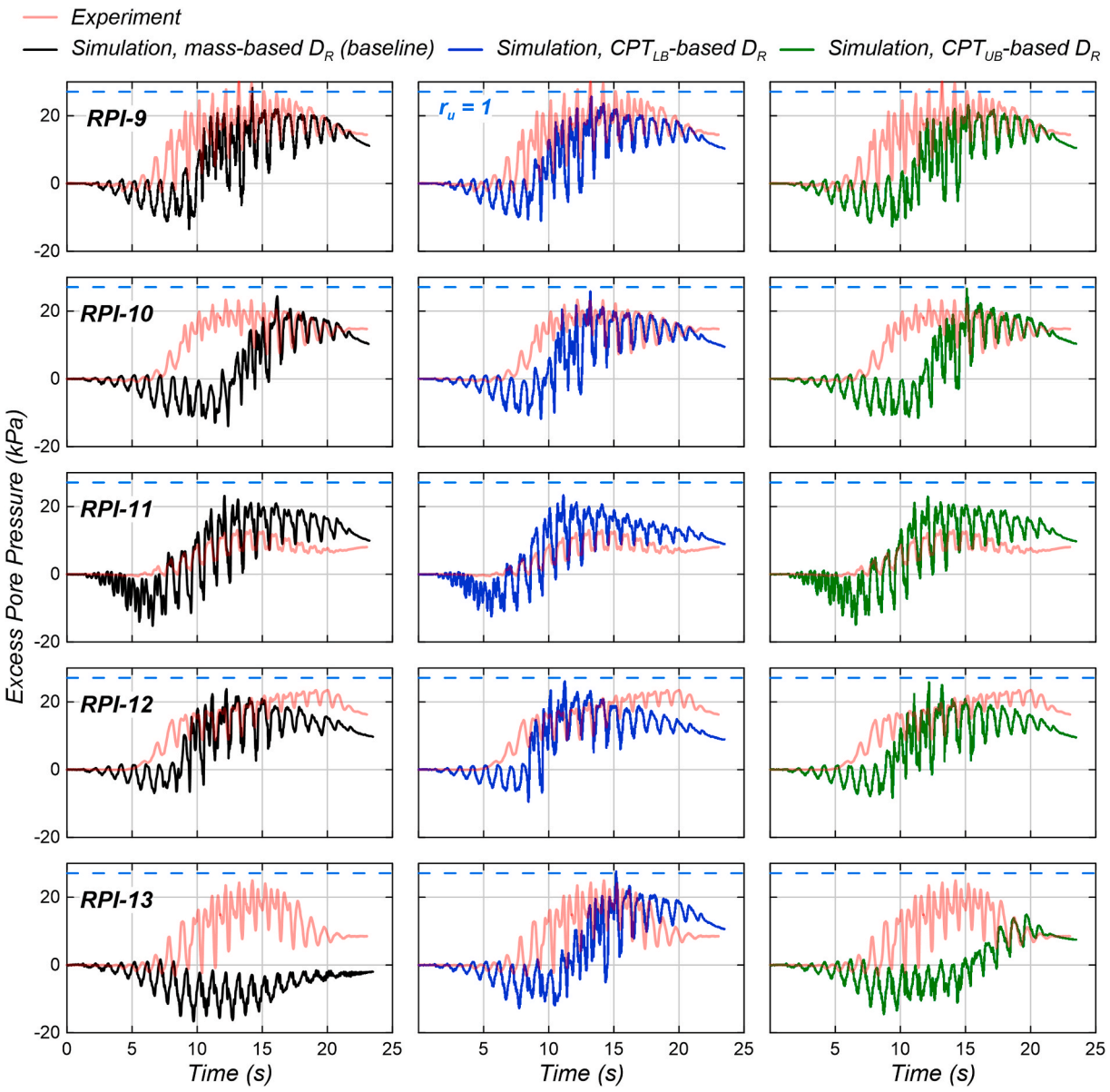

Fig. 12. Excess pore pressure time histories at location PW1 for the RPI tests. Each column corresponds to a different approach for estimating D_R: left column for mass-based D_R, middle column for D_R based on lower bound CPT data, and right column for D_R based on upper bound CPT data.

placement of the sheet-pile wall; and (3) placement of soil layers behind and in front of the wall up to the corresponding soil elevations indicated in Fig. 1. In this scenario, a cohesion of 0.2 kPa, lower than the baseline of 4 kPa, is used for numerical stability. Sensitivity analyses not presented herein showed an important effect of cohesion on the estimated displacements at the end of spinup and using the lowest cohesion that allows for numerical stability is considered appropriate. All other properties are the same as those of the baseline scenario.

The results indicate that the construction process significantly affects the estimated sheet-pile wall displacements at the end of spinup, but only mildly affects the displacements during shaking (Figs. 15 and 16). Note that the experimental displacements reported during shaking did not account for the pre-shaking displacements most likely to isolate the effects of shaking from spinup process and the same was repeated for the simulations. The sheet-pile wall displacement at the end of spinup increases from 2.3 cm (baseline) to 9.4 cm with the alternative construction procedure, which is an increase of around 300%. Contrarily, the incremental displacement at the end of shaking decreases from 82 cm (baseline) to 77 cm with the alternative construction procedure, which is a decrease of 6%. Compared to the experimental displacements, the alternative construction method leads to significant overprediction of the horizontal displacements at the end of spinup (Fig. 15), and a slightly better agreement of displacements at the end of shaking (Fig. 16). As this study was focused on the response at the end of shaking, the construction procedure had a minor effect and either approach is considered reasonable.

It is interesting to note that the numerical construction procedure that is closest to the experimental procedure results in a significant overprediction of wall displacements. The pluviation-based construction procedure resulted in lower stresses near the toe of the wall than the excavation-based procedure, which seems to account for some of the differences between these two approaches. The experimental results fall between these, which may indicate the stress conditions in the centrifuge are intermediate to these two procedures. Neither approach exactly replicates the experimental procedures and the minor effect on final displacements should provide comfort to modelers who may not know or be able to replicate construction procedures used in the field.

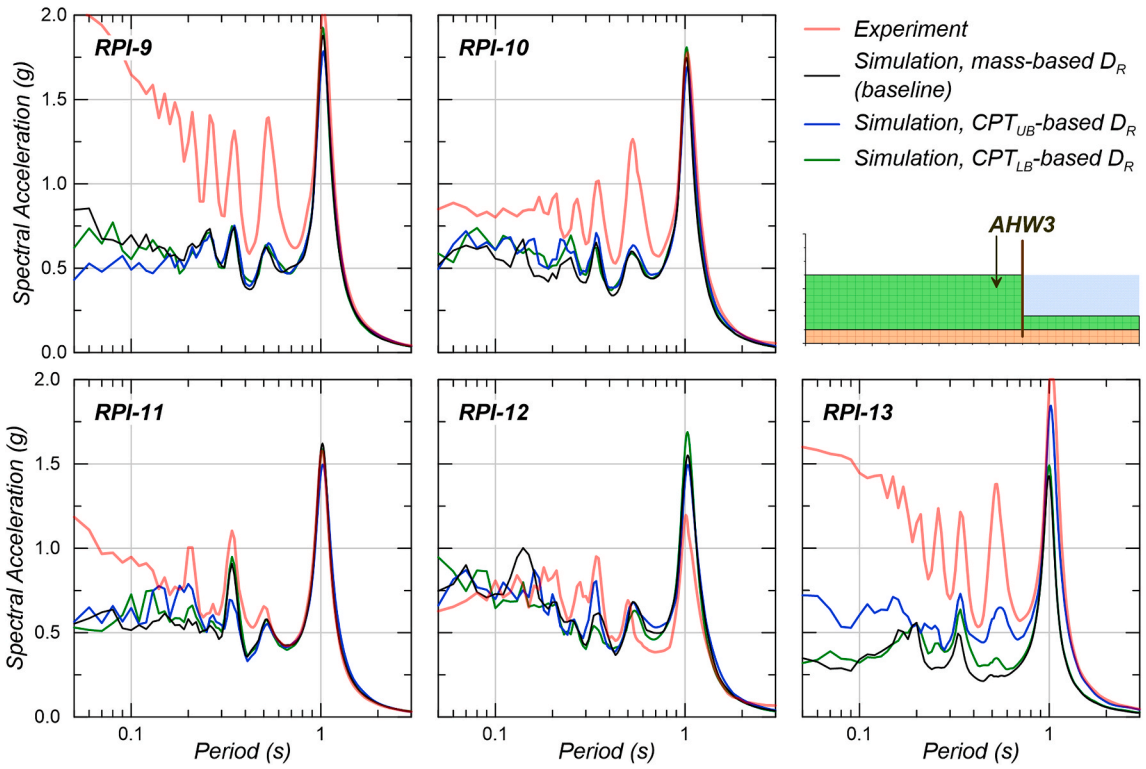

Fig. 13. Response spectra (5% damped) at location AHW3 for the RPI tests and various approaches for estimating D_R.

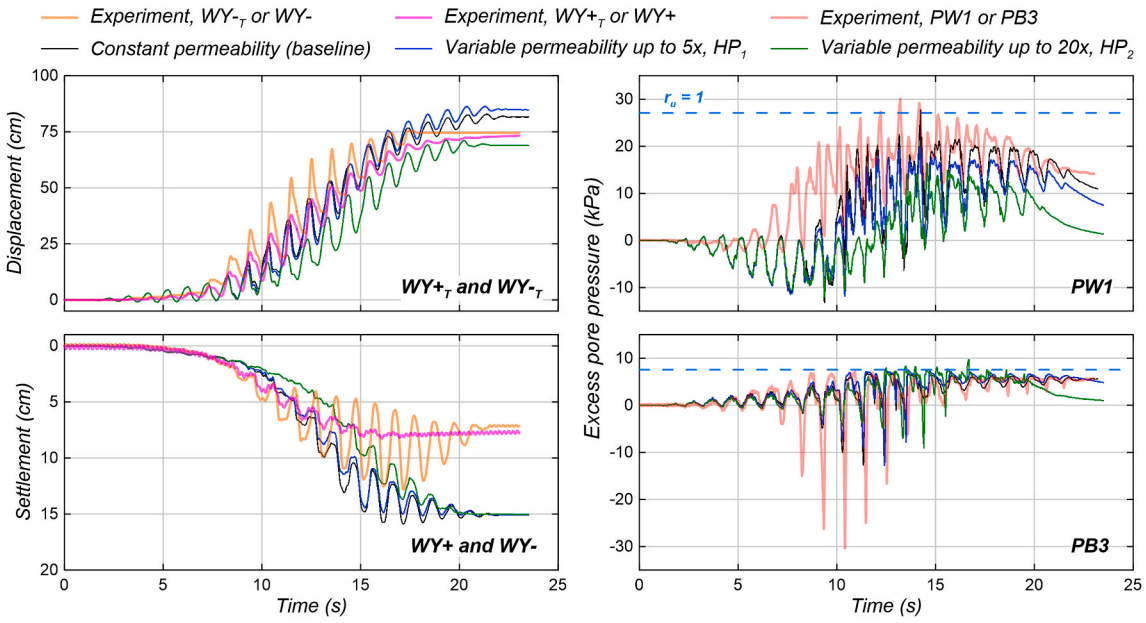

Fig. 14. Effect of permeability on the sheet-pile wall displacements, surface settlement time histories, and excess pore pressure time histories at various locations (Fig. 1).

4.4.2. Effect of soil constitutive model used during model construction

The baseline scenario uses the Mohr-Coulomb constitutive model prior to shaking in order to speed the calculation process. Using different constitutive models for the spinup and shaking phases does not allow for capturing the effect of changes in the soil's state from the onset of the test. Here, the PM4Sand model is used from beginning to end for both the dense and liquefiable soil units. The same PM4Sand parameters calibrated for the shaking phase are used for the spinup phase (Tables 2 and 4).

The results (Figs. 15 and 16) indicate that using a PM4Sand prior to shaking improves the predictions of sheet-pile wall displacements for RPI-9 as displacements increase from 2.3 to 3.5 cm at the end of spinup (Fig. 15), i.e., an increase of about 50%. However, predicted sheet-pile wall displacements at the end of shaking for this scenario are nearly identical to the baseline, with only a very mild increase of 2% (Fig. 16). It is interesting to note that while PM4Sand does a better job of matching the final post-spinup displacement, neither approach is able to match the rate of accumulation of displacement with increasing g level. The Mohr-

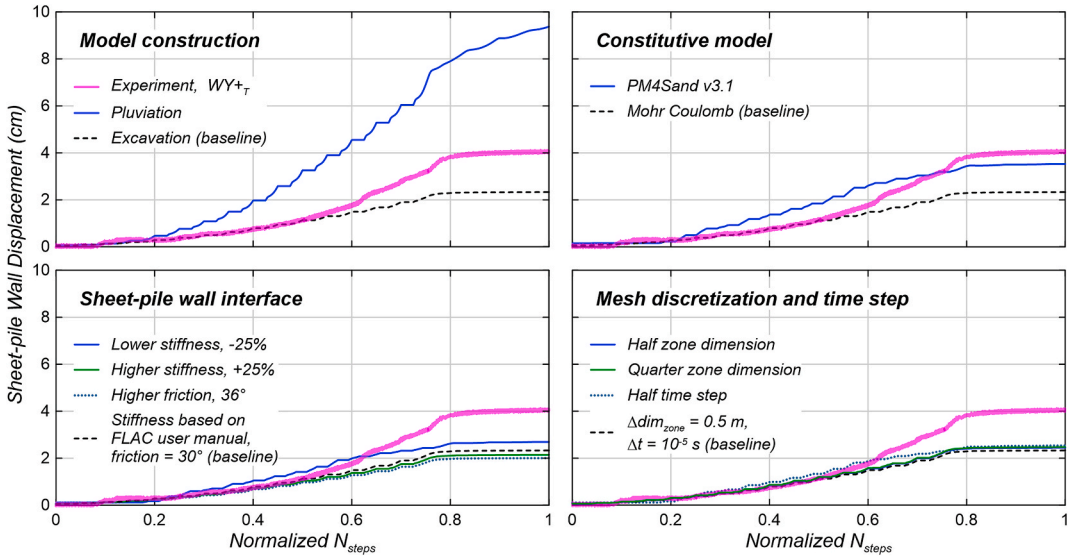

Fig. 15. Effect of various modeling decisions on the sheet-pile wall displacements for RPI-9 during spinup.

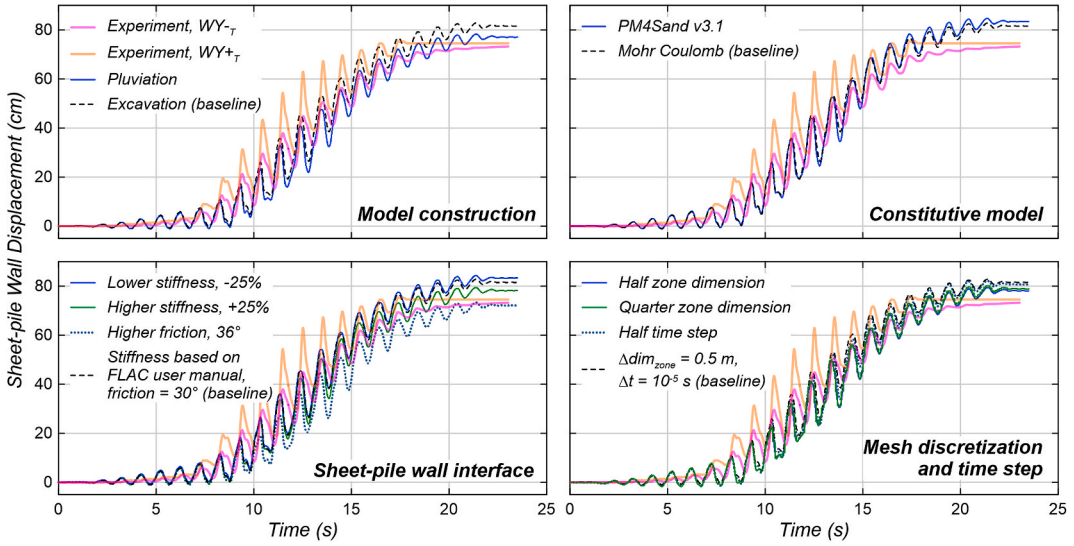

Fig. 16. Effect of various modeling decisions on the sheet-pile wall displacements for RPI-9 during shaking. Note that displacements shown are only for shaking portion of the simulation and do not include displacement during spinup.

Table 2
Relative density estimates from mass-based and CPT-based measurements in the centrifuge tests and corresponding h_{po} values selected for the numerical simulations.

Test	PM4Sand model calibration parameters (liquefiable layer)					
	Mass-based		CPT-based (lower and upper bound values)			
	D_R (%)	h_{po}	D_R (%)	h_{po}	D_R (%)	h_{po}
RPI-9	63	0.072	60	0.095	65	0.065
RPI-10	65	0.065	59	0.105	64	0.068
RPI-11	65	0.065	59	0.105	64	0.068
RPI-12	55	0.138	52	0.168	58	0.11
RPI-13	75	0.038	65	0.065	70	0.048
EU-2	65	0.065	57	0.122	66	0.06
KyU-1	55	0.138	N/A	N/A	N/A	N/A
KyU-3	65	0.065	N/A	N/A	N/A	N/A
KAIST-2	65	0.065	63	0.072	76	0.038
UCD-1	70	0.052	74	0.038	88	0.161
ZJU-1	75	0.038	58	0.11	81	0.045

Table 3
Statistical parameters corresponding to the numerical fit of experimentally recorded wall displacements based on the 11 tests considered in this study.

Parameter	Mass-based D_R	CPT_{LB}-based D_R	CPT_{UB}-based D_R
R^2	0.569	0.577	0.568
Mean bias	2.278	1.029	2.253
Mean square error	13.39	1.40	7.77
Coefficient of variance, COV (bias)	1.32	0.60	0.77

Coulomb model has a similar accumulation to PM4Sand, but with a lower magnitude. Reasons for this discrepancy are unclear, but it is noted that the PM4Sand model calibrations were performed for higher stress levels and for cyclic loading conditions and may not capture the true monotonic behavior of the soil at very low stresses. As discussed for the model construction procedure, neither simulation approach is modeling the true spinup process or soil behavior at very low stresses,

Table 4
Properties of Ottawa F-65 sand utilized in the numerical simulations.

Maximum void ratio, e_{max}	Minimum void ratio, e_{min}	Specific gravity, G_s	Permeability, k (cm/s)
0.78[a]	0.51[a]	2.65[b]	0.012[c]

[a] e_{max} and e_{min} are based on Carey et al. [50].
[b] G_s is based on Vasko et al. [51].
[c] k is based on El Ghoraiby et al. [38].

but disagreements at the end of spinup have a negligible response on the final post-shaking displacements.

4.4.3. Effect of interface properties

The baseline simulation uses stiffness properties for the sheet-pile wall's interface selected following the recommendations provided in the FLAC User Manual and an interface friction angle equal to the critical state friction angle of the soil. Considering that there is no basis or data to guide the selection of these properties, three additional scenarios are considered: (1) an increase of 25% of the interface stiffness; (2) a decrease of 25% of the interface stiffness; and (3) an increase of the friction angle interface from 30° to 36°. Smaller friction angles resulted in instability of the wall during model construction.

The results from the three scenarios in the sheet-pile wall displacements are only modestly different than those from the baseline. Using a higher interface stiffness or friction angle leads to lower displacements by 8–15% at the end of spinup (Fig. 15) and 5–12% at the end of shaking (Fig. 16). Higher stiffness and interface friction angle increase the discrepancies observed between measured and predicted wall displacements at the end of spinup, but improve the agreement at the end of shaking. Lower interface stiffness leads to higher sheet-pile wall displacement by about 15% at the end of spinup, and 2% at the end of shaking. Similar results are obtained from these scenarios for other centrifuge tests (Basu et al. [27]). These results demonstrate that reasonable variations in the interface properties do not significantly affect the model response for this problem. Despite this, having data on the interface properties would still be helpful for selecting the most appropriate values for the simulation.

4.4.4. Effect of model mesh size and time step

The baseline scenario uses a mesh with zones of 0.5 m by 0.5 m along with a time step of 10^{-5} s during shaking. These dimensions and time step are mostly selected for computational efficiency while honoring the minimum requirements for numerical stability of the explicit forward-marching FLAC scheme and the propagation of the input motion frequency content. Simulations for RPI-9 were repeated using meshes with zones that were half (0.25 m by 0.25 m) and one quarter (0.125 m by 0.125 m) as large as the baseline scenario and a timestep that was half as large as the baseline. Simulations using a time step 5×10^{-6} s lead to small variations on the sheet-pile wall displacements both at the end of spinup (Fig. 15), and at the end of shaking (Fig. 16). The effects of time step on excess pore pressure and acceleration responses are also negligible.

The effect of mesh size is more complicated. The smaller meshes had a negligible effect on wall displacements at the end of spinup and a small effect (approximately 5%) on final wall displacements. Simulations using the quarter and half size meshes were almost identical indicating convergence in wall displacement. Fig. 17 shows the effect of mesh size variation on surface settlement, excess pore pressures at sensors PW1 and PD, and acceleration response spectra at AHW3. The change in mesh size had almost no effect on the response spectra or pore pressure response at PD, indicating the baseline mesh was sufficiently small to propagate all frequencies of interest and to provide enough resolution within the dense layer at the bottom of the model. The finer meshes do produce slightly higher settlements (quarter mesh is 4% higher than baseline) and excess pore pressures at the end of shaking at PW1 (quarter mesh is 7% higher than baseline). The final displacements and the excess pore pressures for the baseline and quarter zone size meshes can also be compared by examining the contours in Figs. 4 and 18. The displacements are very similar between the two simulations with the exception of a small gap that opens between the soil and wall in the quarter mesh simulation. The patterns of excess pore pressures are also very similar with significant generation in the upper backfill and dilation near the wall and in the toefill, but differences can be observed near the base of the wall and the ground surface. The finer mesh simulations result in a significant increase in computational time (e.g., 3 times the baseline case when using the 0.25 m mesh and almost 5 times the baseline case when using the 0.125 m mesh), while only producing small differences in the soil response. Therefore, the selected baseline mesh size and time step are deemed to be small enough to provide reasonable results within the soil, while balancing the computational demand.

The change in mesh size has a larger effect on the magnitude of internal stresses within the wall (Fig. 19), although the patterns are very similar between the three meshes. The maximum moment and deformation in the baseline mesh are approximately 5% less than the quarter mesh. The shear force in the baseline mesh is approximately 14% less than the fine mesh, which does show that the baseline mesh may have

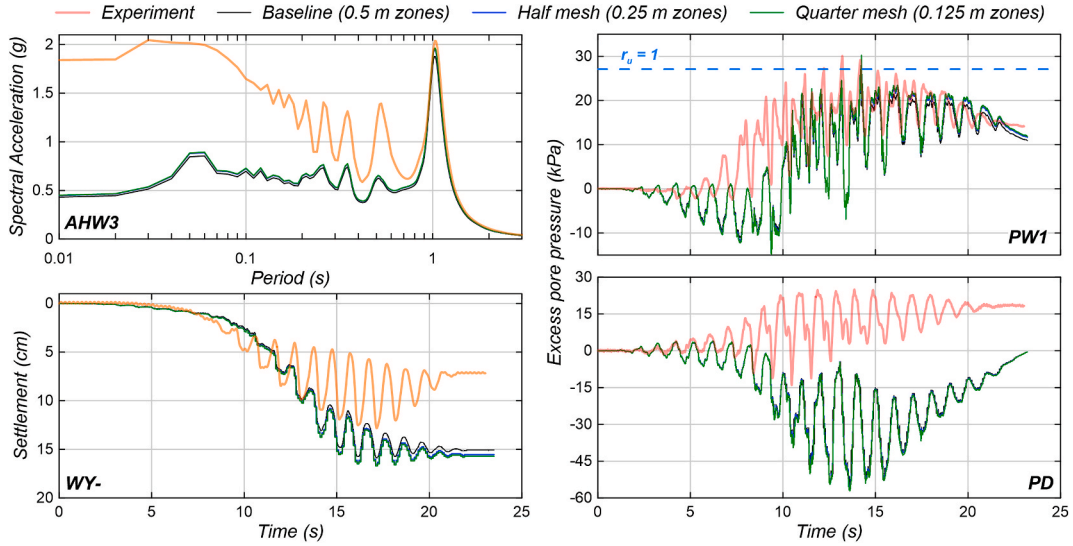

Fig. 17. Effect of mesh size on response spectra at AHW3, settlement at WY-, and excess pore pressures at PW1 and PD for RPI-9 during shaking.

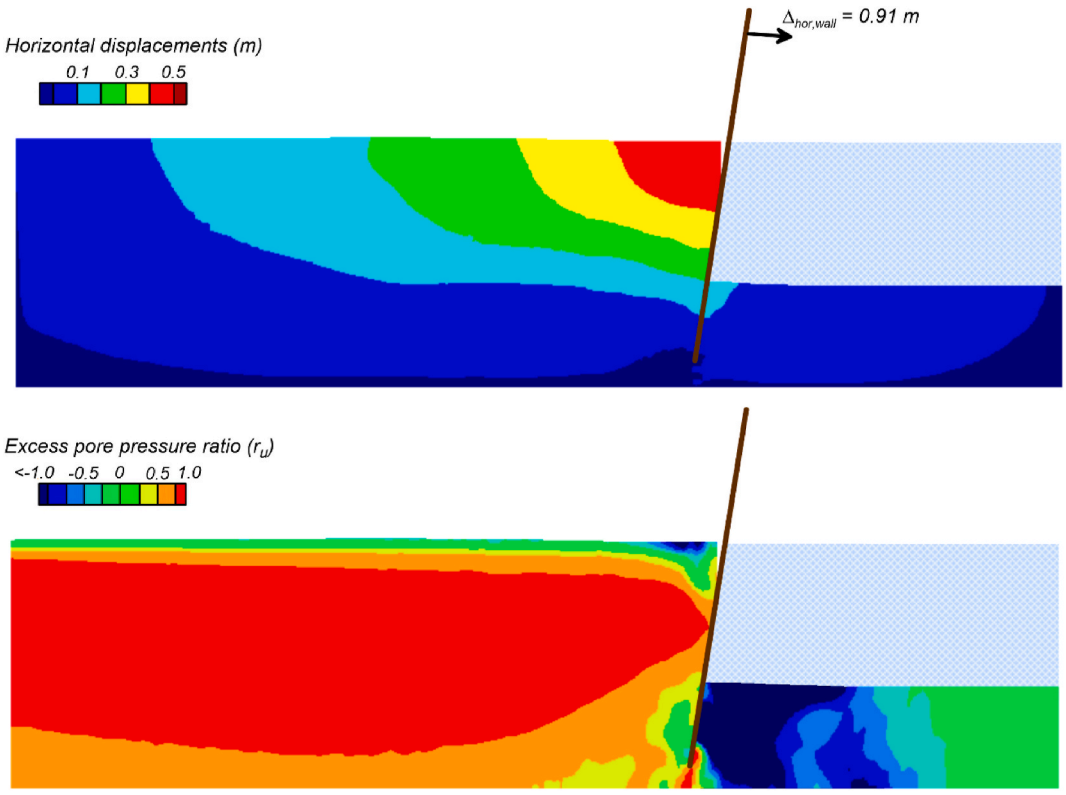

Fig. 18. Contours of horizontal displacements and excess pore pressure ratios at the end of shaking for RPI-9 using 0.125 m zones.

been too coarse to accurately capture the shear distribution within the wall. All of the forces are far below the capacity of the wall, these differences in internal forces are not expected to have a significant effect on the model response, which has been demonstrated in the other results (Figs. 16–18). This analysis does demonstrate that mesh sensitivity should be examined in both the soil and structural response.

5. Discussion

Of the various factors examined in this study, the D_R of the soil was found to be the most critical. This is not surprising as D_R is known to be one of the most important influences on the liquefaction behavior of clean sands. The uncertainty in the D_R achieved within the centrifuge experiments was surprising and the results of this study demonstrated that the CPT-based values did a good job of bracketing the model response for most of the simulations, while the mass-based values tended to underpredict displacements. The discrepancy was most apparent for RPI-13, where the D_R from the lower bound of the CPT profile was 10% lower than the mass-based value and in a much better agreement with the observed displacements. This demonstrates the importance of collecting CPT data during centrifuge models, as is commonly done for field-scale evaluations of liquefaction. The CPT profiles showed significant variability and no attempt was made to directly model that variability in these simulations. This would be an interesting future study.

Model initialization procedures can vary significantly between different numerical analysts, but the effect of these modeling choices is not commonly examined. In this study, two construction procedures and two constitutive models were considered for the stress initiation (spinup) phase of the simulations. These numerical choices did affect the displacement at the end of spinup, but had a very minor effect on the final wall displacement after shaking. This demonstrated that, for the current problem, differences in the initial stresses due to these procedures did not have a significant effect on the numerical model response. This is an important result for forward applications as the true construction process of geotechnical infrastructure is often unknown and difficult to model.

Ground motion variability is one of the largest sources of uncertainty in the seismic response of geotechnical systems. In the current study, the recorded motions from the experiments were known and thus uncertainty in the input motion was not a factor. One of the experiments (RPI-11) changed the motion from the other experiments by reducing the intensity at the predominant frequency (1 Hz) and adding a higher frequency component (3 Hz) to maintain a similar PGA. This change in input motion led to a significant reduction in displacements in the experiment, but not in the simulation. Reasons for this discrepancy are unknown, but this is an area that deserves additional study.

A mesh sensitivity study was performed to determine how the mesh size may have influenced the simulation results. Response metrics such as wall displacement, surface settlement, excess pore pressures at sensor locations, and response spectra generally varied by 5% or less when using meshes with half and one quarter of the size of the baseline simulation. Excess pore pressures and displacement patterns in the soil at the ground surface and near the wall were more affected by using the smaller mesh size. Internal forces in the sheet-pile wall were found to be more affected by using the smaller mesh, with all simulations showing the same patterns, but maximum magnitudes varying between 5 and 17%.

This study has focused on numerical simulations of centrifuge experiments, but several important findings are also likely applicable to simulations of field-scale problems involving retaining walls and liquefaction. First, the study found that simulation results using PM4Sand and FLAC were in reasonable agreement with the suite of centrifuge experiments. The study also found that simulated wall displacements were relatively insensitive to changes in model construction procedures, interface properties, and small variations in the permeability with excess pore pressures (up to five times). It is often challenging to know the “correct” choice for these aspects of the model and the relative insensitivity of the results to these choices provides

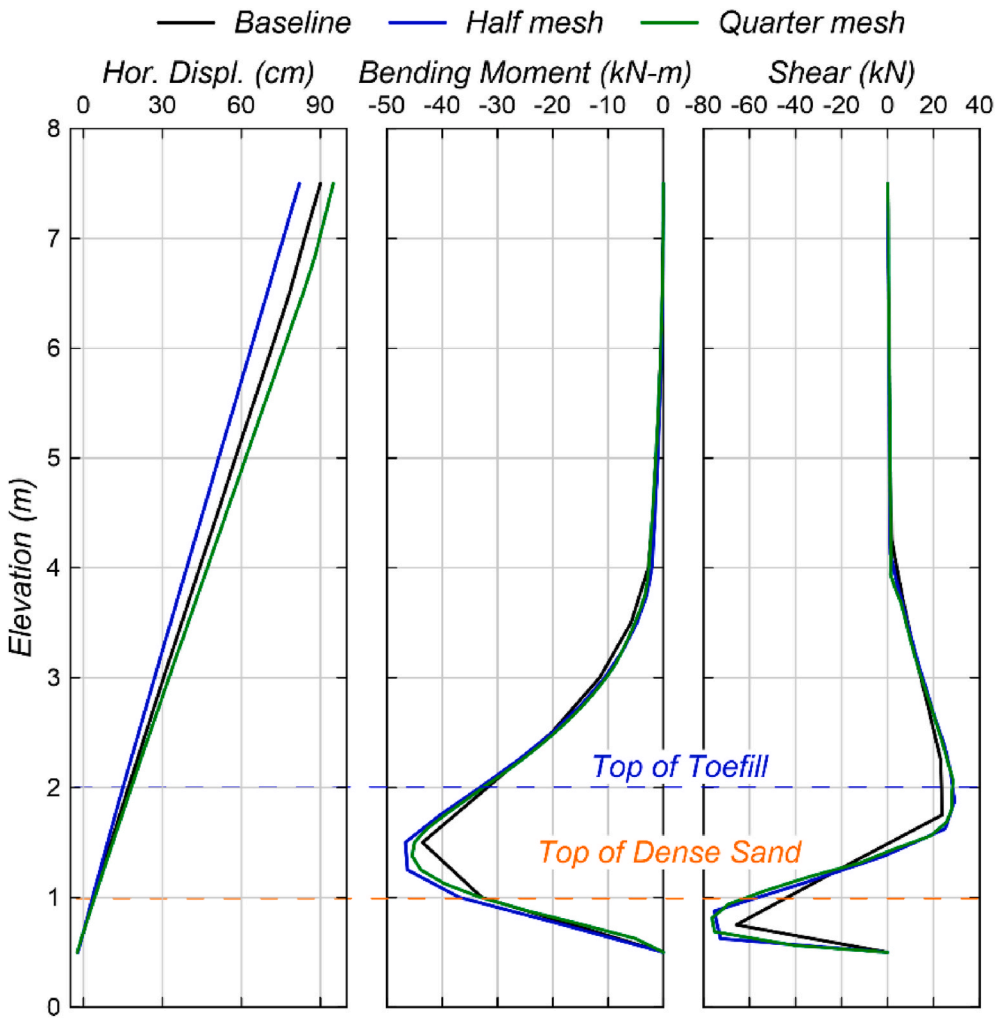

Fig. 19. Effect of mesh size on sheet-pile wall responses at the end of shaking for horizontal displacement, bending moment and shear in the structural elements. The shear force is plotted at the center of element, while bending moments and displacements are plotted at the nodes on each end.

additional confidence. The comparison of experimental and numerical results found that the prediction accuracy varied by as much as a factor of two from the experimental value. Although commonly acceptable and expected for practical purposes and applications, this factor of two in displacement uncertainty is deemed high for an exercise like this one. For this particular problem, much of this uncertainty is attributed to uncertainty in D_R and future studies should place additional effort on constraining the measurements of D_R.

6. Conclusions

This paper presented the results from a numerical study, performed as part of LEAP 2020, that aimed at simulating centrifuge tests of a sheet-pile wall-soil geosystem. Numerical simulations were conducted for centrifuge tests from eleven facilities around the world and the predictions were evaluated in their ability to reasonably capture the observed behaviors and seismic performance. The model consisted of dense and liquefiable layers of Ottawa F-65 sand retained by a sheet-pile wall. The input motions consisted of a pseudo-harmonic excitation applied at the model base as accelerations. The numerical simulations are conducted on the numerical platform FLAC and the soil behavior simulated using the PM4Sand constitutive model. Results are discussed in terms of the sheet-pile wall displacements, surface settlements, excess pore pressures, and spectral accelerations.

A baseline scenario consisting of best-estimate material properties and best modeling practices was first conducted. The results for this scenario showed an overall reasonable agreement of the estimated sheet-pile wall displacements, spectral accelerations near the input motions' fundamental frequency of 1 Hz, and trends of excess porewater pressure for soils with contractive behavior. In contrast, surface settlements were overpredicted, and spectral accelerations at high frequencies were underpredicted. The comparison of the measured and predicted sheet-pile wall displacements for all eleven tests indicated that displacements can generally be predicted with an accuracy that varies from 50 to 200%, i.e., a factor of 2. The baseline results deviated from the experiments in two main areas: (1) an overprediction of wall displacement for a test with a high frequency component in the input motion; and (2) an excessively dilative simulated response (suction) around the bottom of the sheet-pile wall. The reasons for these disagreements are unclear. In addition, the good agreement between the measured and the simulated responses for one metric in a given test (e.g., sheet-pile wall displacements) does not imply that the same level of agreement is achieved for other metrics.

A close evaluation of the relative density (D_R) and permeability of sands provided insight into the importance of these parameters in the prediction of seismic performance of geosystems. Differences in mass-based and CPT-based D_R can be significant, and even though D_R is also expected to vary across the model and with depth, a single representative value was used for the numerical simulations. The system response and displacements were sensitive to D_R of the liquefiable soils

(backfill), as expected. Considering scenarios for both mass-based and CPT-based D_R led to results that enveloped the measured sheet-pile wall displacements for most cases, and results obtained from using the lower bound CPT-based D_R led to the best accuracy. The level of disagreement between the measured and predicted sheet-pile wall displacements is similar to the level of discrepancy between the achieved and targeted mass-based D_R amongst the different experiments (Table 2). Permeability, commonly modeled using a constant value throughout shaking, was herein modeled as variable after liquefaction triggering based on findings from previous studies [18,63]. Changes in permeability led to significant dissipation of excess pore pressures during seismic shaking and minor variations in the sheet-pile wall displacements and surface settlements. A better agreement in terms of sheet-pile wall displacements was obtained for the scenario with variable permeability up to a factor of 5.

In addition to spatial and temporal variability and uncertainties associated with D_R and permeability, the ability of modelers to accurately predict the seismic performance of geosystems is challenged by limitations of the numerical tools and unknown factors inherent to laboratory data. Limitations of the employed numerical tools include using a two-dimensional platform along with a plane-strain constitutive model to simulate the response of sheet-pile wall retaining a liquefiable soil in a rigid box. An implicit assumption in the evaluation of numerical predictions against experiments is that the measured material parameters and the experiment responses are flawless. Factors such as water inflow and movement of sensors during testing could be partially contributing to the discrepancies observed between measured and predicted responses. For instance, it is possible that the water inflow during the experiment suppressed some of the dilation near the bottom of the sheet-pile wall thus reducing some of the dilative behavior that would normally be expected for a sand with $D_R = 90\%$.

This study provides lessons that could guide the performance of similar studies or numerical modeling challenges. The representative value of D_R selected to simulate a centrifuge experiment plays a key role in the system's overall response and the predicted permanent displacements at the end of shaking. Thus, attention should be placed on this parameter and capturing the range of its possible values. Increments of soil permeability post liquefaction triggering play an important role in the amount of excess pore pressure build-up and thus the potential variations of permeability should be considered as a case scenario. Various parametric analyses suggest that the influence of the model construction (stress initialization), 'artificial' cohesion for numerical stability, and the constitutive model used during this phase have a moderate to a significant effect on the predicted pre-shaking displacements. On the other hand, the effect of sheet-pile wall interface's stiffness and friction angle as well as the mesh discretization and time step have a minor effect on pre-shaking displacements. Finally, the effect of all of these aspects on the permanent displacements at the end of shaking is minor. Given this exercise's focus on the final displacements, these results provide confidence that the results presented herein are not overly sensitive to the modeling choices that were made during development of the simulations.

This study suggests that there is always a need for modelers to exercise their models extensively and evaluate the uncertainties imposed by the various numerical choices they make as well as the uncertainties imposed by the various assignments informed by their experimental or field counterparts. Such exercises can help identify the vulnerabilities of each system, better inform soil and site investigation campaigns, and ultimately increase the confidence levels in the results.

Author statement

Devdeep Basu: Conceptualization, Methodology, Formal analysis, Validation, Visualization, Writing- Original draft preparation Renmin Pretell: Conceptualization, Methodology, Formal analysis, Validation, Visualization, Writing- Editing Jack Montgomery: Conceptualization, Methodology, Visualization, Supervision, Writing- Reviewing and Editing Katerina Ziotopoulou: Conceptualization, Visualization, Supervision, Writing- Reviewing and Editing.

Declaration of competing interest

The authors declare that they have no known competing financial interests or personal relationships that could have appeared to influence the work reported in this paper.

Acknowledgements

The authors are grateful to Professors Bruce L. Kutter, Majid Manzari, and Mourad Zeghal, principal investigators of the Liquefaction Experiments and Analyses Project (LEAP) for the invitation to participate in the prediction exercise, and all the participating experimental facilities for providing the data used to conduct this investigation. We thank the two anonymous reviewers for their detailed comments and suggestions for improving this paper. Any opinions, findings, and conclusions or recommendations expressed in this paper are solely those of the authors and do not necessarily reflect any of the institutions and organizations that participated in LEAP 2020.

References

[1] Finn WDL, Byrne PM, Evans S, Law T. Some geotechnical aspects of the Hyogo-ken nanbu (Kobe) earthquake of january 17, 1995. Can J Civ Eng 1996;23:778–96.
[2] Cubrinovski M, Bray JD, Taylor M, Giorgini S, Bradley B, Wotherspoon L, Zupan J. Soil liquefaction effects in the central business district during the february 2011 Christchurch earthquake. Seismol Res Lett 2011;82:893–904.
[3] Ishihara K, Yoshimine M. Evaluation of settlements in sand deposits following liquefaction during earthquakes. Soils Found 1992;32:173–88.
[4] Sento N, Kazama M, Uzuoka R. Experiment and idealization of the volumetric compression characteristics of clean sand after undrained cyclic shear. Dob Gakkai Ronbunshu 2004;2004:307–17.
[5] Zhang G, Robertson PK, Brachman RWI. Estimating liquefaction-induced ground settlements from CPT for level ground. Can Geotech J 2002;39:1168–80.
[6] Yoshimine M, Nishizaki H, Amano K, Hosono Y. Flow deformation of liquefied sand under constant shear load and its application to analysis of flow slide of infinite slope. Soil Dynam Earthq Eng 2006;26:253–64.
[7] Chian SC, Tokimatsu K, Madabhushi SPG. Soil liquefaction–induced uplift of underground structures: physical and numerical modeling. J Geotech Geoenviron Eng 2014;140:04014057.
[8] Dashti S, Bray JD. Numerical simulation of building response on liquefiable sand. J Geotech Geoenviron Eng 2013;139:1235–49.
[9] Ramirez J, Barrero AR, Chen L, Dashti S, Ghofrani A, Taiebat M, Arduino P. Site response in a layered liquefiable deposit: evaluation of different numerical tools and methodologies with centrifuge experimental results. J Geotech Geoenviron Eng 2018;144:04018073.
[10] Ziotopoulou K, Montgomery J, Bastidas AMP, Morales B. Cyclic strength of Ottawa F-65 sand: laboratory testing and constitutive model calibration. In: Geotechnical earthquake engineering and soil dynamics V; 2018. p. 180–9.
[11] Boulanger RW, Ziotopoulou K. On NDA practices for evaluating liquefaction effects. In: Geotechnical earthquake engineering and soil dynamics V; 2018.
[12] Montgomery J, Ziotopoulou K. Numerical simulations of selected LEAP centrifuge experiments with PM4Sand in FLAC. In: Model tests and numerical simulations of liquefaction and lateral spreading; 2020. p. 481–97.
[13] Ziotopoulou K, Montgomery J, Tsiaousi D, Tasiopoulou P, Ugalde J, Travasarou T. Effect of numerical modeling protocols on the seismic response of a liquefiable slope. In: 7th international conference on earthquake engineering; 2019.
[14] Bullock Z, Karimi Z, Dashti S, Porter K, Liel AB, Franke KW. A physics-informed semi-empirical probabilistic model for the settlement of shallow-founded structures on liquefiable ground. Geotechnique 2019;69:406–19.
[15] Beber R, Madabhushi S, Dobrisan A, Haigh S, NMadabhushi S. Leap GWU 2017: investigating different methods for verifying the relative density of a centrifuge model. In: Physical modelling in geotechnics. CRC Press; 2018.
[16] Montgomery J, Ziotopoulou K, Basu D, Pretell R. LEAP 2020 simulation exercise phase I: model calibration. In: Liquefaction analyses and experiments Projects; 2020.
[17] Arulanandan K, Sybico J. Post-liquefaction settlement of sand. In: Proceeding of the wroth memorial symposium; 1992.
[18] Jafarzadeh F, Yanagisawa E. Settlement of sand models under unidirectional shaking. In: First international conference on earthquake geotechnical engineering; 1995. p. 693–8.
[19] Su D, Li X-S, Xing F. Estimation of the apparent permeability in the dynamic centrifuge tests. Geotech Test J 2009;32:22–30.

[20] Wang B, Zen K, Chen GQ, Zhang YB, Kasama K. Excess pore pressure dissipation and solidification after liquefaction of saturated sand deposits. Soil Dynam Earthq Eng 2013;49:157–64.
[21] Manzari M, Kutter B, Zeghal M, Iai S, Tobita T, Madabhushi S, Haigh S, Mejia L, Gutierrez D, Armstrong R, Sharp M, Chen Y-M, Zhou Y-G. LEAP projects: concept and challenges. 2015.
[22] Itasca FLAC.) – fast Lagrangian analysis of continua. 2016., Version 8.0.
[23] Boulanger R, Ziotopoulou K. PM4Sand (Version 3.1): a sand plasticity model for earthquake engineering applications. Davis, CA: University of California; 2017. Report No. UCD/CGM-17/01, Davis.
[24] El Ghoraiby MA, Park H, Manzari MT. Stress-strain behavior and liquefaction strength characteristics of Ottawa F65 sand. Soil Dynam Earthq Eng 2020;138:106292.
[25] Zeghal M. LEAP-RPI 2020, version 0.91 model specifications. 2019.
[26] Kutter B. Dynamic centrifuge modeling of geotechnical structures. In: Transportation research record, TRB. National Research Council; 1992. p. 24–30.
[27] Basu D, Pretell R, Montgomery J, Ziotopoulou K. Numerical simulations of the effects of liquefaction on a retaining wall using PM4Sand and FLAC. In: LEAP-2020 proceedings; 2021 (Under Review).
[28] Dafalias YF, Manzari MT. Simple plasticity sand model accounting for fabric change effects. J Eng Mech 2004;130:622–34.
[29] Boulanger RW. Relating kα to relative state parameter index. J Geotech Geoenviron Eng 2003;129:770–3.
[30] Bolton MD, Gui MW, Garnier J, Corte JF, Bagge G, Laue J, Renzi R. Centrifuge cone penetration tests in sand. Geotechnique 1999;49:543–52.
[31] Sepulveda A, Zeghal M, Kutter B, Manzari M, Abdoun T, Escoffier S, Stuart K, Hung W-Y, Kim D-S, Korre E, Madabhushi G, Manandhar S, Okamura M, Tobita T, Ueda K, Zhou Y-G. Correlations of the CPT and relative density measurements for LEAP-2017 and LEAP-2020 centrifuge tests. 2021.
[32] El Ghoraiby M, Manzari M. Leap 2020: cyclic direct simple shear tests performed at GWU. Dataset: DesignSafe-CI [publisher; 2019. being updated.
[33] El Ghoraiby M, Park H, Manzari M. Leap 2017: soil characterization and element tests for Ottawa F65 sand. Geotech. Report. Washington, DC: The George Washington University; 2017.
[34] Lee M, Gomez M, Kortbawi M, Ziotopoulou K. Examining the liquefaction resistance of lightly cemented sands using microbially induced calcite precipitation (MICP). GeoCongress 2020:53–64. 2020.
[35] Morales B, Ziotopoulou K. Direct simple testing of Ottawa F-65 sand. UC Davis Soil Interactions Laboratory data report; 2018.
[36] Ueda K, Vargas R. LEAP-Asia-2018: stress-strain response of Ottawa F65 sand in cyclic torsional shear tests. DesignSafe-CI [publisher], Dataset, doi:10.17603/DS2D40H.2018.
[37] Vargas RR, Ueda K, Uemura K. Influence of the relative density and K0 effects in the cyclic response of Ottawa F-65 sand - cyclic Torsional Hollow-Cylinder shear tests for LEAP-ASIA-2019. Soil Dynam Earthq Eng 2020;133:106111.
[38] El Ghoraiby M, Park H, Manzari MT. Physical and mechanical properties of Ottawa F65 sand. Cham: Springer International Publishing; 2020. p. 45–67.
[39] Idriss I, Boulanger R. SPT-based liquefaction triggering procedures. 2010. Report No. UCD/CGM-10/02.
[40] Tasiopoulou P, Ziotopoulou K, Humire F, Giannakou A, Chacko J, Travasarou T. Development and implementation of semiempirical framework for modeling postliquefaction shear deformation accumulation in sands. J Geotech Geoenviron Eng 2020;146:04019120.
[41] Parra Bastidas A. Ottawa F-65 sand characterization. Ph.D dissertation. Davis: Department of Civil and Enviropnmental Engineering, University of California; 2016.
[42] Ashwamy A, Sukumaran B, Hoang V. Evaluating the influence of particle shape on liquefaction behavior using discrete element modeling. In: 13th international offshore and polar engineering conference; 2003. p. 542–9. Honolulu, HI, USA.
[43] Dennis ND. In: Donaghe RT, Chaney RC, Silver ML, editors. Influence of specimen preparation techniques and testing procedures on undrained steady state shear strength. West Conshohocken, PA: ASTM International; 1988. p. 642–54.
[44] Lee KL, Seed H. Drained strength characteristics of sands. J Soil Mech Found Div 1967;93:117–41.
[45] Santamarina JC, Cho GC. Determination of critical state parameters in sandy soils—simple procedure. Geotech Test J 2001;24:185–92.
[46] Sasitharan S, Robertson PK, Sego DC, Morgenstern NR. Collapse behavior of sand. Can Geotech J 1993;30:569–77.
[47] Sasitharan S, Robertson PK, Sego DC, Morgenstern NR. State-boundary surface for very loose sand and its practical implications. Can Geotech J 1994;31:321–34.
[48] Sukumaran B, Ashmawy AK. Quantitative characterisation of the geometry of discret particles. Geotechnique 2001;51:619–27.
[49] Carraro JAH, Prezzi M, Salgado R. Shear strength and stiffness of sands containing plastic or nonplastic fines. J Geotech Geoenviron Eng 2009;135:1167–78.
[50] Carey TJ, Stone N, Kutter BL. Grain size analysis and maximum and minimum dry density testing of Ottawa F-65 sand for LEAP-UCD-2017. Cham: Springer International Publishing; 2020. p. 31–44.
[51] Vasko A, El Ghoraiby M, Manzari M. LEAP-GWU-2015 Laboratory tests. DesignSafe-CI [publisher], Dataset, doi:10.17603/DS2TH7Q.2018.
[52] Kuhlemeyer RL, Lysmer J. Finite element method accuracy for wave propagation problems. J Soil Mech Found Div 1973;99:421–7.
[53] Guan X, Madabhushi GSP. Numerical modelling of structures adjacent to retaining walls subjected to earthquake loading. Geosciences 2020;10:486.
[54] Ghosh B, Madabhushi SPG. Centrifuge modelling of seismic soil structure interaction effects. Nucl Eng Des 2007;237:887–96.
[55] Ziotopoulou K. Seismic response of liquefiable sloping ground: class A and C numerical predictions of centrifuge model responses. Soil Dynam Earthq Eng 2018;113:744–57.
[56] Tsiapas Y. Seismic response analysis of liquefiable ground with computational methods. Ph.D. thesis. Athens: Department of Civil Engineering, NTUA; 2017.
[57] Papadimitriou AG, Bouckovalas GD, Dafalias YF. Plasticity model for sand under small and large cyclic strains. J Geotech Geoenviron Eng 2001;127:973–83.
[58] Tsiapas YZ, Bouckovalas GD. Selective filtering of numerical noise in liquefiable site response analyses. In: Geotechnical earthquake engineering and soil dynamics V; 2018. p. 248–57.
[59] Geyin M, Maurer BW. An analysis of liquefaction-induced free-field ground settlement using 1,000+ case histories: observations vs. State-of-Practice predictions. GeoCongress 2019:489–98. 2019.
[60] Chiaradonna A, Ziotopoulou K, Carey T, DeJong J. Cone penetration testing to constrain the calibration process of a sand plasticity model for nonlinear deformation analysis. 2022. CPT'22 Bologna (in press).
[61] Gao G-y, Xie W, Song J, Wang Y. Prediction of seismic compression of saturated sand considering the ground motion characteristics and variable permeability. Soil Dynam Earthq Eng 2020;130:105971.
[62] Tsaparli V, Kontoe S, Taborda DMG, Potts DM. Vertical ground motion and its effects on liquefaction resistance of fully saturated sand deposits. Proc Math Phys Eng Sci 2016;472:20160434.
[63] Shahir H, Pak A, Taiebat M, Jeremić B. Evaluation of variation of permeability in liquefiable soil under earthquake loading. Comput Geotech 2012;40:74–88.
[64] Ueng T-S, Wang Z-F, Chu M-C, Ge L. Laboratory tests for permeability of sand during liquefaction. Soil Dynam Earthq Eng 2017;100:249–56.
[65] Bayoumi A, Karray M, Chekired M. Measurement of Hydraulic conductivity variation in post seismic behavior of sand using TxSS. GeoEdmonton 2018. 2018.
[66] Adamidis O, Madabhushi G. Post-liquefaction reconsolidation of sand. Proc Math Phys Eng Sci 2016;472:20150745.
[67] Basu D, Montgomery J, Stuedlein AW. Observations and challenges in simulating post-liquefaction settlements from centrifuge and shake table tests. Soil Dynam Earthq Eng 2022;153:107089.
[68] Ishihara K. In: Arulanandan K, Scott RF, editors. Review of the predictions for Model 1 in the VELACS program. Rotterdam: A.A. Balkema; 1994. p. 1353–68.